Redundant Manipulator Kinematics and Dynamics on Differentiable Manifolds

Edward J. Haug
Carver Distinguished Professor Emeritus
Department of Mechanical Engineering
The University of Iowa

Adrian Peidro
Assistant Professor
Systems Engineering and Automation Department
Miguel Hernandez University, Spain

7/31/2022

Abstract

A recently published treatment of nonredundant manipulator kinematics and dynamics on differentiable manifolds is extended to kinematically redundant manipulators. Analysis at the configuration level shows that forward kinematics and dynamics of redundant manipulators are identical to that for nonredundant manipulators. The manifold-based inverse kinematics formulation that is presented for redundant manipulators, in contrast, yields parameterizations of set-valued inverse kinematic mappings at the configuration level, where sharper results are obtained than those presented in the literature using velocity formulations. Explicit expressions are derived for set-valued inverse kinematic mappings for both serial and non-serial (called compound) kinematically redundant manipulators, as functions of vectors of arbitrary parameters. Parameterizations are presented for both manipulator regular configuration manifolds and self-motion manifolds, the latter comprised of sets of inputs that map into the same output. It is shown that kinematically redundant configuration manifolds and self-motion differentiable manifolds are distinctly different and play complementary roles in redundant manipulator kinematics. Computational methods are presented for evaluation of set-valued inverse kinematic mappings, without problem dependent ad-hoc analytical manipulations. Redundant serial and compound manipulator examples are presented to illustrate computation of set-valued inverse kinematic mappings and use of self-motion manifold mappings in obstacle avoidance applications. Differentiation of configuration level inverse mappings yields inverse velocity and acceleration mappings as functions of time dependent arbitrary parameters that play a central role in manipulator dynamics and control.

1 Introduction

Nonredundant manipulators have numbers of input and output coordinates equal to the number of degrees of freedom of the underlying mechanism. As a result, except at singular configurations, they have single valued forward and inverse kinematic mappings [1, 2]. In contrast, kinematically redundant manipulators [3, 4] have numbers of input coordinates equal to the number of degrees of freedom of the underlying mechanism, but have fewer output coordinates. This creates a situation in which inverse kinematic mappings are set-valued, providing the control engineer with freedom to plan trajectories in configuration space that avoid obstacles, avoid singularities, or enhance performance of the manipulator. This opportunity comes with attendant analytical complexity associated with the fact that inverse kinematic mappings are set-valued; i.e., for a given output, there are an infinite number of inputs that yield

that output. As a result, the role of differentiable manifolds in kinematics of redundant manipulators is pervasive. In contrast, in the case of nonredundant manipulators, analysis on manipulator configuration manifolds reduces essentially to multivariable calculus [1,2]. A restricted class of redundant manipulators, called *redundant input manipulators*, has inputs greater in number than the number of mechanism degrees of freedom [5]. This category of redundant manipulator is not addressed herein.

Most literature on kinematically redundant manipulators [3, 4] and references cited therein, except for early contributions [6, 7, 8, 9] and recent developments focused on *seven degree of freedom* (7-DOF) serial manipulators [10, 11, 12], deals with manipulator performance at the velocity level where equations are linear in velocities. This leads to a situation in which configurations must be recovered using approximate numerical integration formulas that induce error and numerous other difficulties that are summarized in [11]. In contrast, the treatment presented herein obtains explicit representations for set-valued inverse kinematic mappings at the configuration level that can support obstacle avoidance and other manipulator performance requirements.

A substantial literature deals with 7-DOF redundant serial manipulators that model the human arm and shoulder or involve spray painting and manufacturing functions [10, 11, 12]. Following an early approach that introduced concepts of manifold parameterization [7], inverse kinematic mappings for these specialized 7-DOF manipulators are derived using one of the joint coordinates as an independent parameter. In the independent input parameter approach, all other joint coordinates are derived as problem-dependent expressions, often quite complex, in terms of the independent coordinate. While useful results are obtained for specialized applications, this explicit parameterization approach is not valid for redundant manipulators whose configuration manifold cannot be globally parameterized by a single variable. The differentiable manifold approach presented herein does not rely on existence of a globally valid parameterization or on ad-hoc representation of dependent joint variables as functions of independent joint variables. Instead, it yields a broadly applicable computational formulation that can be implemented in real-time on modern high-speed microprocessors, using only basic results of differential geometry on Euclidean space R^n.

In order to treat set-valued inverse kinematic mappings, except in the case of redundant serial manipulators, the manipulator kinematics formulation must account for mechanism generalized coordinates and associated kinematic constraints. This reality reduces the four categories of nonredundant manipulator treated in [1, 2] to just *redundant serial manipulators* and *redundant compound manipulators*, the latter encompassing a broad spectrum of applications that include high load capacity construction, earth moving, and material handling equipment. As defined herein, compound manipulators include classically defined *parallel manipulators* that are comprised of a single moving platform that is supported by parallel serial chains of actuated joints [13], as well as diverse other manipulator geometries. In short, redundant compound manipulators account for all redundant manipulators that are not serial. As in the case of nonredundant manipulators, regular configuration spaces for both serial and compound kinematically redundant manipulators are shown to be differentiable manifolds. Furthermore, ordinary differential equations (ODE) of dynamics in terms of input coordinates presented in [2] remain valid for kinematically redundant manipulators. However, ODE in output coordinates for kinematically redundant manipulators are not possible.

While set-valued inverse kinematic mappings at the configuration level have recently been derived for specialized 7-DOF serial manipulators [11, 12], no general inverse

configuration mapping approach has been presented. One of the few attempts to construct general parameterizations of inverse kinematic mappings for redundant manipulators was by DeMers and Kreutz-Delgado [9]. They used large sets of input-output data to train neural networks that approximate the inverse mapping. Drawbacks of their approach are that these data span a substantial fraction of the configuration space and that the parameterization obtained is an approximation, without error control. In contrast, the approach presented herein provides a local parameterization with error control, to meet accuracy requirements of diverse applications.

A differential geometric construct is employed herein that yields explicit characterizations of inverse kinematic mappings as functions of vectors of arbitrary (or free) parameters on charts of associated differentiable manifolds for serial and compound kinematically redundant manipulators in Sections 2 and 3, respectively. Analytical complexities associated with kinematically redundant manipulators require local characterization of inverse kinematic mappings on charts that cover the manipulator configuration manifold [14], since global parameterizations of redundant manipulator kinematics are generally not possible. Numerical methods are presented in Appendix A for systematic evaluation of functions involved in analysis on charts, suitable for use in kinematics, dynamics, and control. Inverse kinematic velocity and acceleration mappings that are required for manipulator dynamics and control are presented in Appendices B and C. Finally, conclusions are presented in Section 4.

To make issues associated with kinematically redundant manipulators more precise, it is helpful to consider two elementary examples.

1.1 A Redundant Serial Manipulator

The redundant serial manipulator shown in Fig. 1 has one translational joint and two rotational joints. The mapping from input coordinates $\mathbf{y} \in \mathrm{R}^3$ to output coordinates $\mathbf{z} \in \mathrm{R}^2$ is

$$\mathbf{z} = \mathbf{G}(\mathbf{y}) = \begin{bmatrix} \mathrm{y}_1 + \cos \mathrm{y}_2 + 2\cos(\mathrm{y}_2 + \mathrm{y}_3) \\ \sin \mathrm{y}_2 + 2\sin(\mathrm{y}_2 + \mathrm{y}_3) \end{bmatrix} \tag{1}$$

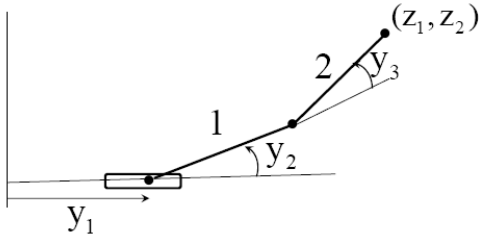

Figure 1 Redundant Serial Manipulator with One Translational and Two Rotational Joints

Since $\mathbf{G}(\mathbf{y})$ is nonlinear in **y**, it is not obvious how to obtain an inverse mapping. To gain insight, the *Jacobian* of $\mathbf{G}(\mathbf{y})$ is the matrix

$$\begin{aligned} \mathbf{G}'(\mathbf{y}) &\equiv \left[\partial \mathrm{G}_\mathrm{i}(\mathbf{y}) / \partial \mathrm{y}_\mathrm{j} \right] \\ &= \begin{bmatrix} 1 & -\sin \mathrm{y}_2 - 2\sin(\mathrm{y}_2 + \mathrm{y}_3) & -2\sin(\mathrm{y}_2 + \mathrm{y}_3) \\ 0 & \cos \mathrm{y}_2 + 2\cos(\mathrm{y}_2 + \mathrm{y}_3) & 2\cos(\mathrm{y}_2 + \mathrm{y}_3) \end{bmatrix} \end{aligned} \tag{2}$$

This 2×3 Jacobian matrix has full row rank if there is a 2×2 nonsingular submatrix, hence a locally defined one parameter inverse kinematic mapping. If the second row is zero, which

occurs if and only if $\cos y_2 = 0$ and $\cos(y_2 + y_3) = 0$, a one parameter inverse mapping fails to exist; i.e., there is no one parameter inverse mapping in a neighborhood of any **y** for which $\cos y_2 = 0$ and $\cos(y_2 + y_3) = 0$. Other than at this family of singularities, the implicit function theorem [15] implies there is a locally valid, one parameter, inverse kinematic mapping.

With the *serial manipulator configuration* defined as $\mathbf{x} = \begin{bmatrix} \mathbf{y}^T & \mathbf{z}^T \end{bmatrix}^T \in R^5$, the manipulator *configuration space* is $X^s = \{\mathbf{x} \in R^5 : \mathbf{G}(\mathbf{y}) - \mathbf{z} = \mathbf{0}\}$ and the *regular configuration space*, in which the manipulator has locally a one parameter inverse kinematic mapping, is

$$\begin{aligned} \tilde{X}^s &= \{\mathbf{x} \in X^s : \cos y_2 \neq 0 \ \textbf{or} \ \cos(y_2 + y_3) \neq 0\} \\ &= \{\mathbf{x} \in X^s : \cos y_2 \neq 0\} \cup \{\mathbf{x} \in X^s : \cos(y_2 + y_3) \neq 0\} \\ &= \{\mathbf{x} \in X^s : \cos y_2 > 0\} \cup \{\mathbf{x} \in X^s : \cos y_2 < 0\} \\ &\quad \cup \{\mathbf{x} \in X^s : \cos(y_2 + y_3) > 0\} \\ &\quad \cup \{\mathbf{x} \in X^s : \cos(y_2 + y_3) < 0\} \\ &\equiv \tilde{X}_1^s \cup \tilde{X}_2^s \cup \tilde{X}_3^s \cup \tilde{X}_4^s \end{aligned} \tag{3}$$

Each $\tilde{X}_i^s$ is path connected. They are not disjoint, however, as seen by configurations $\mathbf{x}^1 = \begin{bmatrix} y_1 & 0 & 0 & y_1 + 3 & 0 \end{bmatrix}^T \in \tilde{X}_1^s \cap \tilde{X}_3^s$, $\mathbf{x}^2 = \begin{bmatrix} y_1 & \pi & 0 & y_1 - 3 & 0 \end{bmatrix}^T \in \tilde{X}_2^s \cap \tilde{X}_4^s$, and $\mathbf{x}^3 = \begin{bmatrix} y_1 & \pi & -\pi & y_1 + 1 & 0 \end{bmatrix}^T \in \tilde{X}_2^s \cap \tilde{X}_3^s$. Even though $\tilde{X}_1^s$ and $\tilde{X}_2^s$ are disjoint, they are connected by a path in $\tilde{X}_3^s$ from $x^1 \in \tilde{X}_1^s \cap \tilde{X}_3^s$ to $x^3 \in \tilde{X}_2^s \cap \tilde{X}_3^s$. Similarly, even though $\tilde{X}_3^s$ and $\tilde{X}_4^s$ are disjoint, they are connected by a path in $\tilde{X}_2^s$ from $x^3 \in \tilde{X}_2^s \cap \tilde{X}_3^s$ to $x^2 \in \tilde{X}_2^s \cap \tilde{X}_4^s$. The union of the four sets is thus path connected. Hence, $\tilde{X}^s$ is comprised of a single, *path connected, singularity free component* [1]. Every pair of configurations $\mathbf{x}^i = \begin{bmatrix} \mathbf{y}^{iT} & \mathbf{z}^{iT} \end{bmatrix}^T$, i = 1, 2, in $\tilde{X}^s$ can thus be connected by one or more singularity free continuous trajectories $\mathbf{x}(t) \in \tilde{X}^s$ such that $\mathbf{x}(0) = \mathbf{x}^1$ and $\mathbf{x}(1) = \mathbf{x}^2$.

It is instructive to compare connectivity of the regular configuration space of the foregoing redundant serial manipulator to that of the nonredundant serial manipulator shown in Fig. 2 that is obtained by eliminating the second bar in the manipulator of Fig. 1. For this manipulator, $\mathbf{y} = \begin{bmatrix} y_1 & y_2 \end{bmatrix}^T \in R^2$, $\mathbf{z} = \begin{bmatrix} z_1 & z_2 \end{bmatrix}^T \in R^2$, and the forward kinematic map is

$$\mathbf{z} = \bar{\mathbf{G}}(\mathbf{y}) = \begin{bmatrix} y_1 + \cos y_2 \\ \sin y_2 \end{bmatrix} \tag{4}$$

with Jacobian $\bar{\mathbf{G}}'(\mathbf{y}) = \begin{bmatrix} 1 & -\sin y_2 \\ 0 & \cos y_2 \end{bmatrix}$ and associated determinant $\left|\bar{\mathbf{G}}'(\mathbf{y})\right| = \cos y_2$.

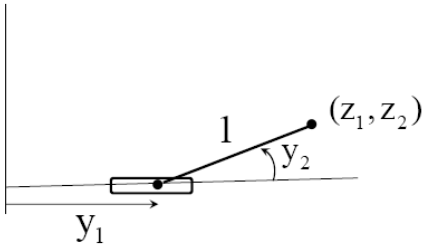

Figure 2 Nonredundant Serial Manipulator

This manipulator has a locally single valued, continuously differentiable inverse kinematic mapping $\mathbf{y} = \bar{\mathbf{G}}^{-1}(\mathbf{z})$ in $X = \left\{ \mathbf{x} = \begin{bmatrix} \mathbf{y}^T & \mathbf{z}^T \end{bmatrix}^T \in R^4 : \bar{\mathbf{G}}(\mathbf{y}) - \mathbf{z} = \mathbf{0} \right\}$, provided $\cos y_2 \neq 0$. The *regular configuration space is* thus $\tilde{X} = \{ \mathbf{x} \in X : \cos y_2 > 0 \} \cup \{ \mathbf{x} \in X : \cos y_2 < 0 \} \equiv \tilde{X}^1 \cup \tilde{X}^2$ where both $\tilde{X}^1$ and $\tilde{X}^2$ are path connected, singularity free sets. In the case of this nonredundant manipulator, $\tilde{X}^1$ and $\tilde{X}^2$ are disjoint and it is impossible to find a singularity free continuous trajectory in X^s between configurations in $\tilde{X}^1$ and $\tilde{X}^2$. The issue of existence of nonsingular paths between configurations within and between components of nonredundant manipulators is discussed at in [1] and references cited therein. Due to the fact that, for a given output in a redundant manipulator, there are in general an infinite number of associated inputs, this issue will require that fundamentally new considerations be addressed for redundant manipulators.

The distinction between the serial manipulators of Figs. 1 and 2 is profound. Adding a third link to the nonredundant manipulator of Fig. 2 yields the redundant manipulator of Fig. 1. Whereas the nonredundant manipulator has disjoint components whose configurations cannot be connected by continuous nonsingular trajectories, every pair of configurations in the regular configuration space of the redundant manipulator can be connected by one or more continuous nonsingular trajectories. This illustrates one of the positive attributes of redundant manipulators.

1.2 A Redundant Compound Manipulator

Two bodies shown in Fig. 3 move in a plane without rotation, connected by a unit length distance constraint. They are located in the plane by generalized coordinates, $\mathbf{q} \in R^3$. Input coordinates $\mathbf{y} \in R^2$ are intended to control the position of body 1 and the vertical coordinate of body 2, which is the output coordinate $z = q_3 \in R^1$. The unit distance constraint between bodies 1 and 2 is represented as the *holonomic constraint equation*

$$\Phi(\mathbf{q}) = \left(q_1^2 + (q_3 - q_2)^2 - 1 \right) / 2 = 0 \tag{5}$$

Inputs are related to generalized coordinates by the *input equation*

$$\mathbf{\Psi}(\mathbf{y}, \mathbf{q}) = \begin{bmatrix} y_1 - q_1 & y_2 - q_2 \end{bmatrix}^T = \mathbf{0} \tag{6}$$

and outputs are related to generalized coordinates by the *output equation*

$$\mathbf{\Gamma}(\mathbf{q}, \mathbf{z}) = z - q_3 = 0 \tag{7}$$

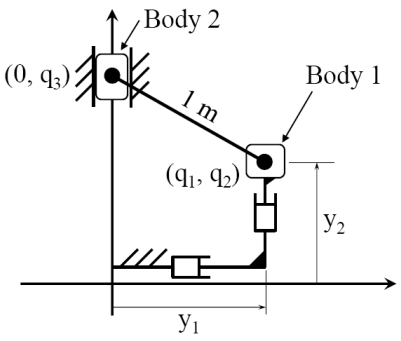

Figure 3 Compound Manipulator with Two Bodies and One Distance Constraint

The Jacobian of the combined constraints of Eqs. (5) and (6) with respect to **q** is

$$\begin{aligned}\mathbf{\Omega_q(y,q)} &= \begin{bmatrix}\Phi(\mathbf{q})\\ \mathbf{\Psi(y,q)}\end{bmatrix}_{\mathbf{q}} = \begin{bmatrix}\Phi_{\mathbf{q}}(\mathbf{q})\\ \mathbf{\Psi_q(y,q)}\end{bmatrix}\\ &= \begin{bmatrix} q_1 & -(q_3-q_2) & (q_3-q_2)\\ -1 & 0 & 0\\ 0 & -1 & 0\end{bmatrix}\end{aligned} \tag{8}$$

With determinant $\left|\mathbf{\Omega_q(y,q)}\right| = q_3 - q_2$. Thus, in a neighborhood of any configuration with $q_3 - q_2 = 0$, there is no continuous forward kinematic mapping from **y** to **q**, hence none from **y** to z. The manipulator *configuration space*, comprised of configurations $\mathbf{x} = \begin{bmatrix}\mathbf{y}^T & \mathbf{q}^T & z\end{bmatrix}^T \in R^6$, is $X^c \equiv \left\{\mathbf{x} \in R^6 : \mathbf{\Psi(y,q)} = \mathbf{0}, \Phi(\mathbf{q}) = 0, \text{ and } \mathbf{\Gamma(q,z)} = \mathbf{0}\right\}$. The manipulator *regular configuration space* is $\tilde{X}^c \equiv \left\{\mathbf{x} \in X^c : \ q_3 - q_2 \neq 0\right\}$, which is partitioned into *disjoint components* $\tilde{X}^+ \equiv \left\{\mathbf{x} \in R^6 : \mathbf{\Psi(y,q)} = \mathbf{0}, \Phi(\mathbf{q}) = 0, \mathbf{\Gamma(q,z)} = \mathbf{0}, \text{ and } (q_3 - q_2) > 0\right\}$ and $\tilde{X}^- \equiv \left\{\mathbf{x} \in R^6 : \mathbf{\Psi(y,q)} = \mathbf{0}, \Phi(\mathbf{q}) = 0, \mathbf{\Gamma(q,z)} = \mathbf{0}, \text{ and } (q_3 - q_2) < 0\right\}$. From Eq. (5), $q_3 - q_2 = \pm\sqrt{1 - q_1^2} \neq 0$ in $\tilde{X}^c$. With $q_1 \equiv v$, which is arbitrary in the range $-1 < v < 1$, the relation $q_3 - q_2 = \pm\sqrt{1 - v^2}$ and Eqs. (6) and (7) yield one parameter inverse kinematic mappings in each of the components, $\mathbf{y}^{\pm} = \left[\begin{array}{cc} v & z - \left(\pm\sqrt{1-v^2}\right)\end{array}\right]^T$ and $\mathbf{q}^{\pm} = \left[\begin{array}{ccc} v & z - \left(\pm\sqrt{1-v^2}\right) & z\end{array}\right]^T$. These mappings provide information that enables planning a trajectory $\mathbf{x}(t) = \begin{bmatrix}\mathbf{y}^T(t) & \mathbf{q}^T(t) & \bar{z}(t)\end{bmatrix}^T$, for a specified output $\bar{z}(t)$, to avoid obstacles.

The foregoing situation, in which the regular configuration space is partitioned into disjoint components, throughout which continuous forward kinematic mappings and set-valued inverse kinematic mappings exist, is typical of redundant compound manipulators. It leads to more intricate conditions for regular behavior of redundant compound manipulators than arise in the case of redundant serial manipulators.

As a simple illustration of obstacle avoidance using the free parameter v in the set-valued inverse kinematic mapping $\mathbf{q}^{\pm} = \begin{bmatrix} v & z - \left(\pm\sqrt{1-v^2}\right) & z \end{bmatrix}^T$, a nominal configuration trajectory is defined in X^+ by v = 0, with output $\bar{z}(t) = q_3(t) = t,\ 0 \le t \le 1$. Using the inverse mappings $\mathbf{y}^{\pm}$ and $\mathbf{q}^{\pm}$, one may select $\mathbf{y}(t) = \begin{bmatrix} 0 & t-1 \end{bmatrix}^T$ and $\mathbf{q}(t) = \begin{bmatrix} 0 & t-1 & t \end{bmatrix}^T$. If an obstacle defined by the inequality $q_2 \ge -1/2$ is imposed, the foregoing generalized coordinate trajectory $q_2(t) = t - 1$ penetrates the obstacle for $0 \le t < 1/2$. Setting $q_2(t) = t - \left(\sqrt{1-v^2}\right) = -1/2$, for $0 \le t < 1/2$, to avoid penetrating the obstacle, $v = \sqrt{1-(t+1/2)^2}$. The value of v = 0 is retained for $1/2 \le t \le 1$. The value of $\bar{z}(t)$ over the entire period $0 \le t \le 1$ is not changed by this so-called *self-motion transformation*, but new input and generalized coordinates are obtained from Eqs. (5) and (6),

$$\hat{\mathbf{y}}(t) = \begin{bmatrix} \sqrt{1-(t+1/2)^2} \\ -1/2 \end{bmatrix}, 0 \le t < 1/2;$$

$$\hat{\mathbf{y}}(t) = \begin{bmatrix} 0 \\ t-1 \end{bmatrix}, 1/2 \le t \le 1$$

$$\hat{\mathbf{q}}(t) = \begin{bmatrix} \sqrt{1-(t+1/2)^2} \\ -1/2 \\ t \end{bmatrix}, 0 \le t < 1/2;$$

$$\hat{\mathbf{q}}(t) = \begin{bmatrix} 0 \\ t-1 \\ t \end{bmatrix}, 1/2 \le t \le 1$$

which avoid penetration of the obstacle. This selection of the free parameter in the inverse kinematic mapping yields inputs and generalized coordinates that retain the desired output trajectory $\bar{z}(t) = t$, while avoiding penetration of the obstacle. It is shown in Section 3 that such explicit analytical computation is generally not possible in realistic applications, but algorithms based on differentiable manifold theory are presented to avoid obstacles.

2 Kinematically Redundant Serial Manipulators

A *serial manipulator* is defined as a chain of bodies connected by single degree of freedom joints in which input coordinates define transformations from inboard bodies to adjacent outboard bodies and determine the configurations of all bodies in the chain. The *vector of input coordinates* in joints of the manipulator is denoted $\mathbf{y} \in R^n$. The last body in the chain is called the *end-effector*. Some or all configuration coordinates of the end-effector comprise the *vector of output coordinates* $\mathbf{z} \in R^m$. If $n > m$, the manipulator is said to be a *kinematically redundant serial manipulator* and the *forward kinematic mapping* is the input-output equation

$$\mathbf{z} = \mathbf{G}(\mathbf{y}) \tag{9}$$

where $\mathbf{G}: R^n \to R^m$ is k-times continuously differentiable, $k \ge 2$. The first task in redundant serial manipulator kinematics is to characterize the *set-valued inverse mapping* $\mathbf{G}^{-1}: R^m \to R^n$,

$$\mathbf{G}^{-1}(\mathbf{z}) = \left\{ \mathbf{y} \in \mathrm{R}^{n} : \mathbf{G}(\mathbf{y}) = \mathbf{z} \right\} \tag{10}$$

2.1 Serial Manipulator Configuration Space

To characterize the inverse mapping $\mathbf{G}^{-1}$, it is first necessary to define the serial manipulator configuration space. With $\mathbf{x} = \begin{bmatrix} \mathbf{y}^{T} & \mathbf{z}^{T} \end{bmatrix}^{T} \in \mathrm{R}^{n+m}$ defined as *manipulator configuration coordinates*, the *serial manipulator configuration space* is the set $\mathrm{X}^{s} = \left\{ \mathbf{x} \in \mathrm{R}^{n+m} ; \mathbf{z} = \mathbf{G}(\mathbf{y}) \right\}$. Provided the Jacobian $\mathbf{G}'(\mathbf{y}) \equiv \left[\partial \mathrm{G}_{i}(\mathbf{y}) / \partial \mathrm{y}_{j} \right]_{m \times n}$ has full row rank at $\bar{\mathbf{y}}$, there is an $m \times m$ nonsingular submatrix of $\mathbf{G}'(\bar{\mathbf{y}})$. Let $\breve{\mathbf{y}} \in \mathrm{R}^{m}$ be comprised of input coordinates corresponding to columns of this submatrix and $\hat{\mathbf{y}} \in \mathrm{R}^{n-m}$ be comprised of the remaining input coordinates. Provided $\bar{\mathbf{x}} \in \mathrm{X}^{s}$, the implicit function theorem [15] assures there is a unique differentiable solution of $\mathbf{G}(\breve{\mathbf{y}}, \hat{\mathbf{y}}) = \mathbf{z}$, $\breve{\mathbf{y}} = \mathbf{w}(\mathbf{z}, \hat{\mathbf{y}})$, for all $(\mathbf{z}, \hat{\mathbf{y}})$ in a neighborhood of $(\bar{\mathbf{z}}, \hat{\bar{\mathbf{y}}})$; i.e., an n – m parameter family of local solutions of $\mathbf{G}(\mathbf{y}) = \mathbf{z}$ for fixed **z**, characterized by $\hat{\mathbf{y}}$. There is no assurance, however, that such a solution is valid over all of X^{s}. If $\mathrm{rank}(\mathbf{G}'(\bar{\mathbf{y}})) < m$, there is no such family of solutions throughout any neighborhood of $\bar{\mathbf{y}}$, in which case $\bar{\mathbf{x}}$ is called *singular*.

2.2 Regular Serial Manipulator Configuration Space

To avoid singular configurations, the *regular serial manipulator configuration space* is defined as $\tilde{\mathrm{X}}^{s} = \left\{ \mathbf{x} \in \mathrm{X}^{s} : \mathrm{rank}(\mathbf{G}'(\mathbf{y})) = m \right\} = \left\{ \mathbf{x} \in \mathrm{X}^{s} : \left| \mathbf{G}'(\mathbf{y}) \mathbf{G}'^{T}(\mathbf{y}) \right| > 0 \right\}$. This is an open subset of X^{s} in the relative topology, so it is comprised of a finite number of *maximal, disjoint, path connected, singularity free components* $\tilde{\mathrm{X}}_{i}^{s}$, such that $\tilde{\mathrm{X}}_{i}^{s} \cap \tilde{\mathrm{X}}_{j}^{s} = \varphi$ if $i \neq j$ and $\cup_{i} \tilde{\mathrm{X}}_{i}^{s} = \tilde{\mathrm{X}}^{s}$, where φ is the empty set [16]. With local parameterizations $\breve{\mathbf{y}} = \mathbf{w}_{i}(\mathbf{z}, \hat{\mathbf{y}})$, $\tilde{\mathrm{X}}^{s}$ is a *differentiable manifold* and the $\tilde{\mathrm{X}}_{i}^{s}$ are *submanifolds*.

2.3 Serial Manipulator Inverse Kinematic Configuration Mapping

In early literature focused on characterizing the set-valued inverse kinematic mapping of Eq. (10) [6, 8, 9], concepts of differential geometry were used to address the problem at the configuration level. Subsequently, an extensive literature has focused almost exclusively on redundant manipulator analysis at the velocity level, where equations are linear in velocities. While useful results have been obtained with velocity analysis, information at the configuration level is lost [11]. The purpose of this section is to employ differential geometry to analytically and computationally characterize the set-valued inverse mapping of Eq. (10) at the configuration level.

As shown in Section 2.2, for $\bar{\mathbf{x}} \in \tilde{\mathrm{X}}^{s}$, there exists an $n - m$ parameter inverse configuration mapping in a neighborhood of $\bar{\mathbf{x}}$. To characterize such a mapping, define

$$\mathbf{U} = \mathbf{G}'^{T}(\bar{\mathbf{y}}) \tag{11}$$

and use *singular value decomposition* to evaluate a solution **V** of

$$\mathbf{G}'(\bar{\mathbf{y}})\mathbf{V} = \mathbf{0} \quad \mathbf{V}^{T}\mathbf{V} = \mathbf{I} \tag{12}$$

where the column rank of **U** is m and that of **V** is n – m [17]. Thus, the columns of **U** and **V** span R^n and any $\mathbf{y} \in \mathbf{G}^{-1}(\mathbf{z}) \subset \mathrm{R}^n$ may be represented in the form

$$\mathbf{y} = \bar{\mathbf{y}} + \mathbf{V}\mathbf{v} - \mathbf{U}\mathbf{u} \tag{13}$$

Note that at $\mathbf{y} = \bar{\mathbf{y}}$, $\bar{\mathbf{v}} = \mathbf{0}$ and $\bar{\mathbf{u}} = \mathbf{0}$. The condition that **y** of Eq. (13) is in $\mathbf{G}^{-1}(\mathbf{z})$ is

$$\mathbf{G}(\bar{\mathbf{y}} + \mathbf{V}\mathbf{v} - \mathbf{U}\mathbf{u}) - \mathbf{z} = \mathbf{0} \tag{14}$$

The Jacobian of the left side of Eq. (14) with respect to **u**, at $\bar{\mathbf{x}}$; i.e., at $\mathbf{v} = \mathbf{0}$, $\mathbf{u} = \mathbf{0}$, and $\mathbf{z} = \bar{\mathbf{z}}$, is $-\mathbf{G}'(\bar{\mathbf{y}})\mathbf{U} = -\mathbf{U}^{\mathrm{T}}\mathbf{U}$, which is nonsingular. Thus, the implicit function theorem [15] implies Eq. (14) has a unique continuously differentiable solution $\mathbf{u} = \mathbf{h}(\mathbf{v}, \mathbf{z})$ for **u** as a function of **v** and **z** in a neighborhood of $(\mathbf{v}, \mathbf{z}) = (\mathbf{0}, \bar{\mathbf{z}})$; i.e.,

$$\mathbf{y}(\mathbf{v}, \mathbf{z}) = \bar{\mathbf{y}} + \mathbf{V}\mathbf{v} - \mathbf{U}\mathbf{h}(\mathbf{v}, \mathbf{z}) \tag{15}$$

2.4 The Regular Serial Manipulator Configuration Differentiable Manifold

Defining $\mathbf{w} = \begin{bmatrix} \mathbf{z}^{\mathrm{T}} & \mathbf{v}^{\mathrm{T}} \end{bmatrix}^{\mathrm{T}} \in \mathrm{R}^n$ and $\bar{\mathbf{w}} = \begin{bmatrix} \bar{\mathbf{z}}^{\mathrm{T}} & \mathbf{0} \end{bmatrix}^{\mathrm{T}}$, Eq. (15) is the one-to-one differentiable mapping $\mathbf{y}(\mathbf{v}, \mathbf{z}) = \bar{\mathbf{y}} + \mathbf{V}\mathbf{v} - \mathbf{U}\mathbf{h}(\mathbf{v}, \mathbf{z}) \equiv \boldsymbol{\psi}(\mathbf{w})$. Multiplying Eq. (13) on the left by $\mathbf{V}^{\mathrm{T}}$ and using Eq. (12), $\mathbf{v} = \mathbf{V}^{\mathrm{T}}(\mathbf{y} - \bar{\mathbf{y}})$. Using this result and Eq. (9), $\mathbf{w} = \begin{bmatrix} \mathbf{G}^{\mathrm{T}}(\mathbf{y}) & (\mathbf{y} - \bar{\mathbf{y}})^{\mathrm{T}}\mathbf{V} \end{bmatrix}^{\mathrm{T}} \equiv \boldsymbol{\phi}(\mathbf{y})$, which is a one-to-one differentiable mapping. This shows that $\mathbf{y} = \boldsymbol{\psi}(\boldsymbol{\phi}(\mathbf{y}))$ and $\boldsymbol{\psi}^{-1} = \boldsymbol{\phi}$. Thus, Eq. (15) provides a continuously differentiable parameterization of $\tilde{\mathrm{X}}^{\mathbf{s}}$ in a neighborhood N of $\mathbf{w} = \bar{\mathbf{w}}$. This neighborhood and the mapping of Eq. (15) that are assured by the implicit function theorem define a *chart* on $\tilde{\mathrm{X}}^{\mathbf{s}}$. Creating a family of such charts to cover $\tilde{\mathrm{X}}^{\mathbf{s}}$ provides an *atlas* that defines $\tilde{\mathrm{X}}^{\mathbf{s}}$ as a *differentiable manifold* with disjoint, maximal, path connected, singularity free components $\tilde{\mathrm{X}}_{\mathrm{i}}^{\mathbf{s}}$ [14].

Analytical relations that characterize differentiable manifolds are defined locally on open sets N^{i} as parameterizations $\mathbf{y} = \boldsymbol{\psi}^{\mathrm{i}}(\mathbf{w}) \equiv \bar{\mathbf{y}} + \mathbf{V}\mathbf{v} - \mathbf{U}\mathbf{h}(\mathbf{v}, \mathbf{z})$ of Eq. (15) on N^{i}. The set N^{i} and mapping $\boldsymbol{\psi}^{\mathrm{i}}(\mathbf{w})$ is called a *chart*, denoted $(\mathrm{N}^{\mathrm{i}}, \boldsymbol{\psi}^{\mathrm{i}}(\mathbf{w}))$. A family of charts, called an *atlas*, is defined to cover $\tilde{\mathrm{X}}^{\mathbf{s}}$; i.e., $\cup_{\mathrm{i}} \mathrm{N}^{\mathrm{i}} = \tilde{\mathrm{X}}^{\mathbf{s}}$, such that the mappings $\boldsymbol{\psi}^{\mathrm{i}}$ are compatible [14]. Kinematic analysis on a component $\tilde{\mathrm{X}}_{\mathrm{i}}^{\mathbf{s}}$ of $\tilde{\mathrm{X}}^{\mathbf{s}}$ must therefore be carried out on individual charts and transitioned to adjacent charts as manipulator configurations progress along a trajectory in $\tilde{\mathrm{X}}_{\mathrm{i}}^{\mathbf{s}}$, as shown schematically in Fig. 4.

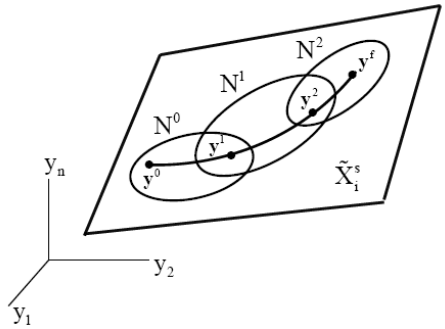

Figure 4 Trajectory Along Charts in $\tilde{X}_i^s$

This *piecewise smooth* form of analysis will be illustrated in mapping components of serial and compound manipulator manifolds. Piecewise analysis shown in Fig. 4 is unavoidable, since, in general, there is no globally valid parameterization $\boldsymbol{\psi}^i(\mathbf{w})$ on a component $\tilde{X}_i^s$ of regular configuration space. As elegantly explained by Hirsch [18], this attribute of differentiable manifold theory that transforms local to global properties of sets and mappings is one of its greatest contributions. The unavoidable reality is that one must adopt local manifold parameterizations, since no global parameterization generally exists.

For use in kinematic analysis and trajectory planning in a component $\tilde{X}_i^s$, partial derivatives of $\mathbf{h}(\mathbf{v},\mathbf{z})$ and $\mathbf{y}(\mathbf{v},\mathbf{z})$ with respect to **v** and **z** are needed. With $\mathbf{u}=\mathbf{h}(\mathbf{v},\mathbf{z})$, Eq. (14) is the identity $\mathbf{G}(\bar{\mathbf{y}}+\mathbf{V}\mathrm{v}-\mathbf{U}\mathbf{h}(\mathbf{v},\mathbf{z}))-\mathbf{z}=\mathbf{0}$ in variables **v** and **z**. Taking partial derivatives of this identity with respect to **v** and **z**, evaluated at $\mathbf{y}=\bar{\mathbf{y}}+\mathbf{V}\mathrm{v}-\mathbf{U}\mathbf{h}(\mathbf{v},\mathbf{z})$, yields

$$\begin{aligned}\mathbf{G}'(\mathbf{y})\left(\mathbf{V}-\mathbf{U}\mathbf{h}_{\mathrm{v}}\right)&=\mathbf{0}\\ \mathbf{G}'(\mathbf{y})\left(-\mathbf{U}\mathbf{h}_{\mathrm{z}}\right)-\mathbf{I}&=\mathbf{0}\end{aligned}\tag{16}$$

At $\mathbf{y}=\bar{\mathbf{y}}$, from Eq. (11), $\mathbf{G}'(\bar{\mathbf{y}})\mathbf{U}=\mathbf{U}^{\mathrm{T}}\mathbf{U}$ is nonsingular, so define $\mathbf{B}(\bar{\mathbf{y}})=\left(\mathbf{U}^{\mathrm{T}}\mathbf{U}\right)^{-1}$. Since $\mathbf{G}'(\mathbf{y})$ is a continuously differentiable function of **y**,

$$\mathbf{B}(\mathbf{y})\equiv\left(\mathbf{G}'(\mathbf{y})\mathbf{U}\right)^{-1}\tag{17}$$

is well defined and continuously differentiable in a neighborhood of $\mathbf{y}=\bar{\mathbf{y}}$. Thus, Eqs. (16) yield

$$\begin{aligned}\mathbf{h}_{\mathrm{v}}(\mathbf{v},\mathbf{z})&=\mathbf{B}(\mathbf{y})\mathbf{G}'(\mathbf{y})\mathbf{V}\\ \mathbf{h}_{\mathrm{z}}(\mathbf{v},\mathbf{z})&=-\mathbf{B}(\mathbf{y})\end{aligned}\tag{18}$$

Applying these results to $\mathbf{y}(\mathbf{v},\mathbf{z})$ of Eq. (15),

$$\begin{aligned}\mathbf{y}_{\mathrm{v}}(\mathbf{v},\mathbf{z})&=\mathbf{V}-\mathbf{U}\mathbf{B}(\mathbf{y}(\mathbf{v},\mathbf{z}))\mathbf{G}'(\mathbf{y}(\mathbf{v},\mathbf{z}))\mathbf{V}\\ \mathbf{y}_{\mathrm{z}}(\mathbf{v},\mathbf{z})&=\mathbf{U}\mathbf{B}(\mathbf{y}(\mathbf{v},\mathbf{z}))\end{aligned}\tag{19}$$

The derivatives of Eqs. (18) and (19) enable redundant serial manipulator applications such as obstacle avoidance, singularity avoidance, and dynamic performance optimization.

2.5 The Serial Manipulator Self-Motion Manifold

For fixed $\mathbf{z}=\bar{\mathbf{z}}$, with $\bar{\mathbf{x}}\in\tilde{X}^s$, the mapping of Eq. (15) reduces to

$$\mathbf{y}(\mathbf{v},\bar{\mathbf{z}})=\bar{\mathbf{y}}+\mathbf{V}\mathrm{v}-\mathbf{U}\mathbf{h}(\mathbf{v},\bar{\mathbf{z}})\tag{20}$$

for all **v** in a neighborhood of **0**. For a sequence $\bar{\mathbf{y}}_{\mathrm{j}}\in\mathrm{R}^{\mathrm{n}}$, this yields

$\mathrm{N}^{\mathrm{j}}(\bar{\mathbf{z}})=\left\{\mathbf{y}=\bar{\mathbf{y}}_{\mathrm{j}}+\mathbf{V}\mathbf{v}-\mathbf{U}\mathbf{h}(\mathbf{v},\bar{\mathbf{z}}),\text{ for all }\mathbf{v}\text{ in a neighborhood of }\mathbf{0}\right\}$, whose union $\cup_{\mathrm{j}}\mathrm{N}^{\mathrm{j}}(\bar{\mathbf{z}})$ is a differentiable manifold $\mathbf{Y}^{\mathrm{s}}(\bar{\mathbf{z}})$ in the input space. This manifold is called the *self-motion manifold*, since it is a set of inputs, all of which have forward kinematic mappings onto the same output $\bar{\mathbf{z}}$. The inverse kinematic mapping of Eq. (20) is a parameterization of the self-motion

manifold $\mathbf{Y}^s(\bar{\mathbf{z}})$. Thus, $\mathbf{Y}^s(\bar{\mathbf{z}})$ is a set of inputs that all yield output $\bar{\mathbf{z}}$, some of which may have attractive properties such as avoiding obstacles and singularities. As with all differentiable manifolds, $\mathbf{Y}^s(\bar{\mathbf{z}})$ may be partitioned into maximal disjoint, connected, components $\mathbf{Y}_i^s(\bar{\mathbf{z}})$; i.e., $\mathbf{Y}^s(\bar{\mathbf{z}})$ is, in general, not a connected set.

If $\bar{\mathbf{z}}_i$ and $\bar{\mathbf{z}}_j$ are adjacent outputs in a neighborhood of $\bar{\mathbf{z}}$, one may select vastly different $\bar{\mathbf{y}}_i \in \mathbf{Y}_i^s(\bar{\mathbf{z}}_i)$ and $\bar{\mathbf{y}}_j \in \mathbf{Y}_j^s(\bar{\mathbf{z}}_j)$, so the resulting $\bar{\mathbf{x}}_i$ and $\bar{\mathbf{x}}_j$ are distinctly different in $\tilde{\mathrm{X}}^s$. If one wishes to maintain manipulator configuration continuity in the manifold $\tilde{\mathrm{X}}^s$, uncorrelated large excursions in $\mathbf{Y}^s(\bar{\mathbf{z}})$, with $\mathbf{z} = \bar{\mathbf{z}}$ fixed, must be avoided. In short, the manipulator regular configuration manifold $\tilde{\mathrm{X}}^s$ and the self-motion manifold $\mathbf{Y}^s(\bar{\mathbf{z}})$ are fundamentally different.

2.6 Mapping One-Dimensional Serial Manipulator Self-Motion Manifold Components

To map a self-motion manifold component $\mathbf{Y}_i^s(\bar{\mathbf{z}})$, in case $n - m = 1$, beginning at a configuration $\bar{\mathbf{x}} = \left[\bar{\mathbf{y}}^T \quad \bar{\mathbf{z}}^T\right]^T \in \tilde{\mathrm{X}}_i^s$ that satisfies Eq. (9), the output $\bar{\mathbf{z}}$ is held fixed during the process of mapping $\mathbf{Y}^s(\bar{\mathbf{z}})$, as follows:

(1) At $\mathbf{y} = \bar{\mathbf{y}}$, $v^0 = 0$, use Eqs. (11) and (12) to evaluate $\mathbf{U}$ and $\mathbf{V}$, and evaluate $\mathbf{B}^0 = \mathbf{B}(\bar{\mathbf{y}}) = \left(\mathbf{U}^T\mathbf{U}\right)^{-1}$.

(2) Confirm that $\left|\mathbf{G}'(\mathbf{y})\mathbf{G}'(\mathbf{y})^T\right|$ is positive throughout $\mathbf{Y}_i^s(\bar{\mathbf{z}})$, to avoid crossing a singularity and entering a different component $\mathbf{Y}_j^s(\bar{\mathbf{z}})$.

(3) For a step h > 0 in v, define $v^1 = h$ and obtain $\mathbf{h}(\mathbf{v}^1, \bar{\mathbf{z}})$ using the iterative process of Eq. (62), with $\mathbf{\Lambda}$ replaced by $\mathbf{G} - \mathbf{z}$ and $\mathbf{B} = \mathbf{B}^0$, for $\mathbf{u}^1 = \mathbf{h}(\mathbf{v}^1, \bar{\mathbf{z}})$.

(4) Evaluate $\mathbf{y}^1 = \bar{\mathbf{y}} + \mathbf{V}\mathbf{v}^1 - \mathbf{U}\mathbf{h}(\mathbf{v}^1, \bar{\mathbf{z}})$ from Eq. (15).

(5) Use the iterative process of Eq. (61), with $\mathbf{\Lambda}$ replaced by $\mathbf{G} - \mathbf{z}$, to evaluate $\mathbf{B}^1$.

(6) At $v^k = kh$, $k = 2,\ldots$, evaluate $\mathbf{h}(\mathbf{v}^k, \bar{\mathbf{z}})$ as $\mathbf{u}^k = \mathbf{h}(\mathbf{v}^k, \bar{\mathbf{z}})$ from Eq. (62), with $\mathbf{\Lambda}$ replaced by $\mathbf{G} - \mathbf{z}$, and $\mathbf{B} = \mathbf{B}^{k-1}$, $\mathbf{y}^k = \bar{\mathbf{y}} + \mathbf{V}\mathbf{v}^k - \mathbf{U}\mathbf{h}(\mathbf{v}^k, \bar{\mathbf{z}})$ of Eq. (15).

(7) Evaluate $\mathbf{B}^k$ using the iterative process of Eq. (61), with $\mathbf{\Lambda}$ replaced by $\mathbf{G} - \mathbf{z}$.

(8) Confirm $\left|\mathbf{G}'(\mathbf{y}^k)\mathbf{G}'(\mathbf{y}^k)^T\right|$ is positive and that the sign of $\left|\mathbf{G}'(\mathbf{y}^k)\mathbf{U}\right|$ is invariant in $\mathbf{Y}_i^s(\bar{\mathbf{z}})$, to have $\mathbf{y}^k \in \mathbf{Y}_i^s(\bar{\mathbf{z}})$.

(9) If the condition number [17] of $\mathbf{G}'(\mathbf{y}^k)\mathbf{U}$ is within tolerance, continue the mapping process.

(10) Otherwise, redefine $\bar{\mathbf{y}} = \mathbf{y}^k$, retain $\mathbf{z} = \bar{\mathbf{z}}$, use Eqs. (11) and (12) to evaluate new $\mathbf{U}$ and $\mathbf{V}$, reset $v^0 = 0$, evaluate $\mathbf{B}^0 = \left(\mathbf{U}^T\mathbf{U}\right)^{-1}$, index $v^k = kh$, and continue the mapping process.

This process implements the chart-to-chart continuation process outlined in Section 2.4 and shown schematically in Fig. 4.

As an illustration of a self-motion manifold with disjoint components, consider the two-bar mechanism shown in Fig. 5. The vertical coordinate of point P is the output coordinate, so

$$z = G(\mathbf{y}) = \sin y_1 + \sin(y_1 + y_2) \tag{21}$$

with Jacobian

$$G'(\mathbf{y}) = \begin{bmatrix} \cos y_1 + \cos(y_1 + y_2) & \cos(y_1 + y_2) \end{bmatrix} \tag{22}$$

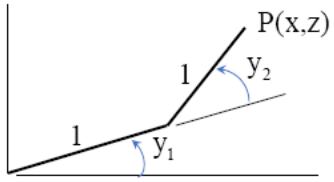

Figure 5 Two-Bar Manipulator

With $\mathbf{x} \equiv \begin{bmatrix} y_1 & y_2 & z \end{bmatrix}^T$, at configuration $\bar{\mathbf{x}} = \begin{bmatrix} 0 & 0 & 0 \end{bmatrix}^T$, $G'(\bar{\mathbf{y}}) = \begin{bmatrix} 2 & 1 \end{bmatrix} \neq \mathbf{0}$. For self-motion mapping, beginning at $\bar{\mathbf{x}}$ and holding $\bar{z} = 0$, $\mathbf{U} = \begin{bmatrix} 2 & 1 \end{bmatrix}^T$ and $\mathbf{V} = (1/\sqrt{5})\begin{bmatrix} -1 & 2 \end{bmatrix}^T$. From Eq. (15), $\mathbf{y} = \begin{bmatrix} -v/\sqrt{5} - 2u & 2v/\sqrt{5} - u \end{bmatrix}^T$. Substituting this into Eq. (21), $-\sin(v/\sqrt{5} + 2u) + \sin(v/\sqrt{5} - 3u) = 0$, so (1) $v/\sqrt{5} + 2u = v/\sqrt{5} - 3u$ and $u = 0$ or (2), using the identity $\sin\alpha = \sin(\pi - \alpha)$, $v/\sqrt{5} + 2u = \pi - v/\sqrt{5} + 3u$ and $u = 2v/\sqrt{5} - \pi$. In case (1), the self-motion mapping is $\mathbf{y} = (v/\sqrt{5})\begin{bmatrix} -1 & 2 \end{bmatrix}^T$, with $G'(\mathbf{y}) = \cos(\mathbf{v}/\sqrt{5})\begin{bmatrix} 2 & 1 \end{bmatrix}$, which is zero if and only if $v = \pm\sqrt{5}\pi/2$. This self-motion mapping, in the range $-\sqrt{5}\pi/2 < v < \sqrt{5}\pi/2$, is the slanted line segment on the left of Fig. 6, which is a component of the self-motion manifold. In case (2), the self-motion mapping is $\mathbf{y} = \begin{bmatrix} -5v/\sqrt{5} + 2\pi & \pi \end{bmatrix}$, with $G'(\mathbf{y}) = \cos(5v/\sqrt{5})\begin{bmatrix} 0 & -1 \end{bmatrix}$, which is zero if and only if $5v/\sqrt{5} = \pm\pi/2$, or $v = \pm\sqrt{5}\pi/10$. The self-motion mapping in the range $-\sqrt{5}\pi/10 < v < \sqrt{5}\pi/10$ has $y_2 = \pi$ and $-\pi/2 < y_1 < \pi/2$. This is the upper horizontal line in Fig.6, which is a component of the self-motion manifold.

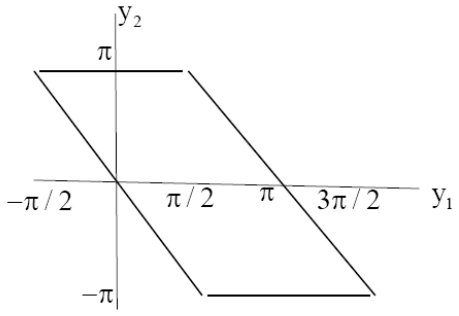

Figure 6 Disjoint Components of Self-Motion Manifold with $\bar{z} = 0$

At configuration $\bar{\mathbf{x}} = \begin{bmatrix} 3\pi & 0 & 0 \end{bmatrix}^T$, $G'(\bar{\mathbf{y}}) = \begin{bmatrix} -2 & -1 \end{bmatrix} \neq \mathbf{0}$. For self-motion mapping, beginning at $\bar{\mathbf{x}}$ and holding $\bar{z} = 0$, $\mathbf{U} = \begin{bmatrix} -2 & -1 \end{bmatrix}^T$ and $\mathbf{V} = (1/\sqrt{5})\begin{bmatrix} 1 & -2 \end{bmatrix}^T$. From Eq. (15),

$\mathbf{y} = \begin{bmatrix} 3\pi + v/\sqrt{5} + 2u & -2v/\sqrt{5} + u \end{bmatrix}^T$. Substituting this into Eq. (21), $\sin(3\pi + v/\sqrt{5} + 2u) + \sin(3\pi - v/\sqrt{5} + 3u) = 0$. Using trigonometric identities, this reduces to $\sin(v/\sqrt{5} + 2u) - \sin(v/\sqrt{5} - 3u) = 0$, so (3) $v/\sqrt{5} + 2u = v/\sqrt{5} - 3u$ and $u = 0$ or (4), using the identity $\sin\alpha = \sin(\pi - \alpha)$, $v/\sqrt{5} + 2u = \pi - v/\sqrt{5} + 3u$ and $u = 2v/\sqrt{5} - \pi$. In case (3), the self-motion mapping is $\mathbf{y} = \begin{bmatrix} \pi + v/\sqrt{5} & -2v/\sqrt{5} \end{bmatrix}^T$, with $G'(\mathbf{y}) = \cos(\mathbf{v}/\sqrt{5})\begin{bmatrix} -2 & -1 \end{bmatrix}$, which is zero if and only if $v = \pm\sqrt{5}\pi/2$. This self-motion mapping, in the range $-\sqrt{5}\pi/2 < v < \sqrt{5}\pi/2$, is the slanted line segment on the right of Fig. 6, which is a component of the self-motion manifold. In case (4), the self-motion mapping is $\mathbf{y} = \begin{bmatrix} 5v/\sqrt{5} + \pi & -\pi \end{bmatrix}^T$, with $G'(\mathbf{y}) = \cos(5v/\sqrt{5})\begin{bmatrix} 0 & 1 \end{bmatrix}$, which is zero if and only if $5v/\sqrt{5} = \pm\pi/2$, or $v = \pm\sqrt{5}\pi/10$. This self-motion mapping in the range $-\sqrt{5}\pi/10 < v < \sqrt{5}\pi/10$ has $y_2 = -\pi$ and $\pi/2 < y_1 < 3\pi/2$. This is the lower horizontal line in Fig. 6, which is a component of the self-motion manifold.

Self-motion mappings with $\bar{z} = 0$ in this example yield a self-motion manifold with disjoint components. With other values of $\bar{z}$, the self-motion manifold consists of a single component in the same range of y_1. For example, with $\bar{\mathbf{x}} = \begin{bmatrix} 0 & \pi/2 & 1 \end{bmatrix}^T$, $G'(\bar{\mathbf{y}}) = \begin{bmatrix} 1 & 0 \end{bmatrix} \neq \mathbf{0}$, $\mathbf{U} = \begin{bmatrix} 1 & 0 \end{bmatrix}^T$ and $\mathbf{V} = \begin{bmatrix} 0 & 1 \end{bmatrix}^T$. From Eq. (15), $\mathbf{y} = \begin{bmatrix} -u & \pi/2 + v \end{bmatrix}^T$. Substituting this into Eq. (21) with $\bar{z} = 1$, $\sin(-u) + \sin(-u + \pi/2 + \mathbf{v}) = 1$, or $f(u,v) = -\sin(u) + \sin(-u + \pi/2 + \mathbf{v}) - 1 = 0$. Since u = v = 0 is a solution of this equation and, at these values, $f_u(0,0) = -\cos 0 - \cos(\boldsymbol{\pi}/2) = 1$, $f(u,v) = 0$ can be numerically solved for u as a function of v on a grid of values of v. The result is substituted into $\mathbf{y} = \begin{bmatrix} -u & \pi/2 + v \end{bmatrix}^T$ and plotted as a single closed curve in the **y**-plane shown in Fig. 7.

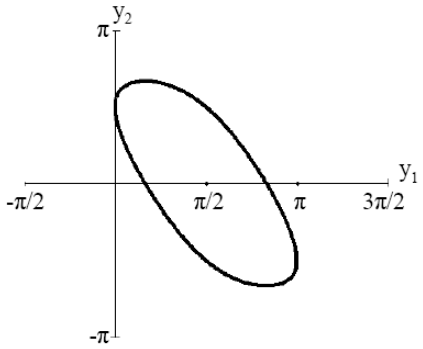

Figure 7 Single Component Self-Motion Manifold with $\bar{z} = 1$

2.7 A Large Scale Redundant Serial Manipulator

To illustrate the foregoing formulation with a large scale manipulator, the inverse kinematic mapping of a generic 7-DOF serial manipulator with seven revolute joints, defined by Denavit-Hartenberg (DH) parameters [19] in Table 1, is computed. The DH parameter transformation between reference frames attached to links i and i-1 is as follows:

(a) $z_0 \ldots z_6$ are the axes of the seven revolute joints

(b) θ_i is the rotation about axis z_{i-1} to make axis x_{i-1} parallel to axis x_i

(c) d_i is the translation along axis z_{i-1} to make axis x_{i-1} coincident with axis x_i

(d) a_i is the translation along axis x_i to make the origins of both frames coincident

(e) α_i is the rotation about axis x_i to make axis z_{i-1} coincident with axis z_i

All joints are of revolute type, so angles θ_i are input coordinates y_i, with offsets shown in the second column of Table 1. The design parameters of this manipulator (d_i, a_i, and α_i) are generic. This means that, unlike most industrial serial manipulators, the axes of successive joints of the manipulator are not subject to special relations (perpendicularity, parallelism, intersection, null link offset, etc) that simplify its kinematics. This 7R serial manipulator is illustrated in Fig. 8 at its home configuration, with $y_i = 0$, i = 1,…,7.

Table 1. DH parameters of a Generic 7-DOF Revolute Serial Manipulator

Frame i-1 to i	θ_i (rad)	d_i (m)	a_i (m)	α_i (rad)
$0 \rightarrow 1$	$y_1 + 0.0779$	0.34720	0.28996	-2.1364
$1 \rightarrow 2$	$y_2 - 0.1052$	-0.31939	-0.252	-3.5813
$2 \rightarrow 3$	$y_3 - 0.1437$	0.3600	-0.4538	-1.1741
$3 \rightarrow 4$	$y_4 - 0.2941$	-0.3534	0.3260	0.6745
$4 \rightarrow 5$	$y_5 + 0.2321$	-0.25974	0.4102	-0.7619
$5 \rightarrow 6$	$y_6 - 0.1586$	0.21070	0.19289	2.6738
$6 \rightarrow 7$	$y_7 + 0.3050$	-0.24998	0.23925	0.9863

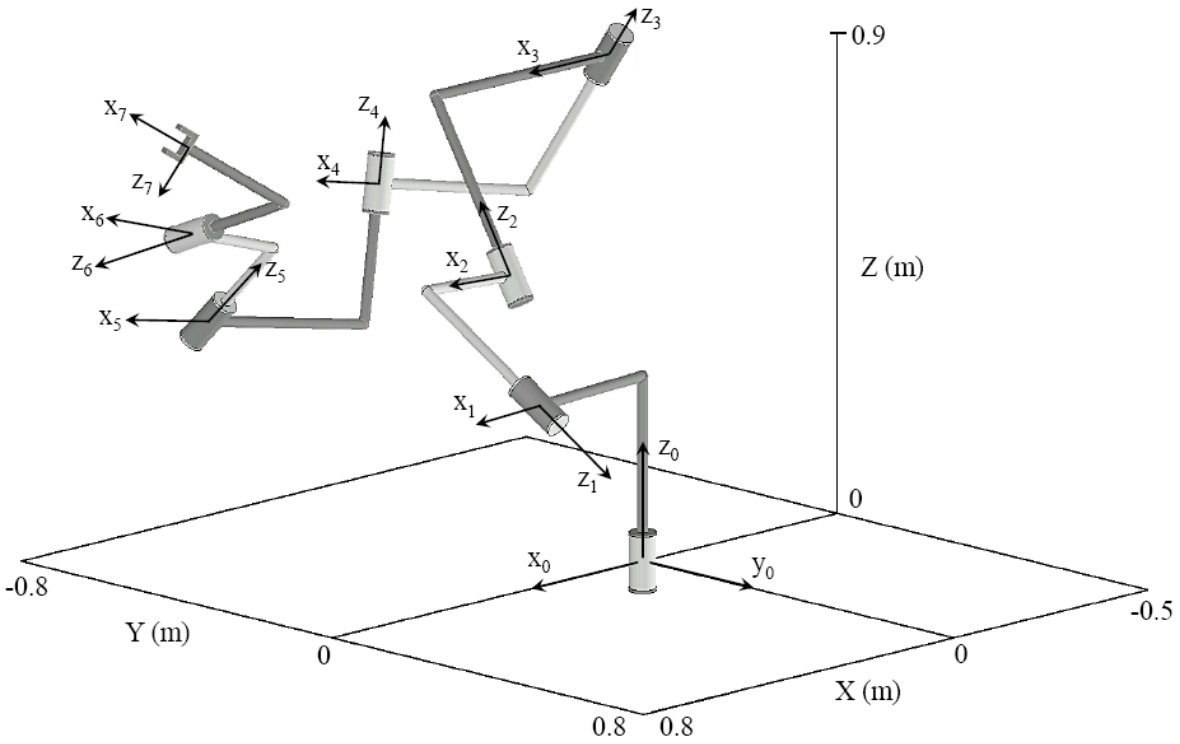

Figure 8 Schematic Representation of Generic 7R Robot in its Home Configuration

Forward kinematics of this manipulator are computed using the DH method [19], which multiplies the following homogeneous transformation matrices from the base frame to the end-effector frame:

$$
{}^{0}\mathbf{T}_{7}\left(\mathbf{y}\right)=\prod_{i=1}^{7}{}^{i-1}\mathbf{T}_{i}\left(y_{i}\right)
$$

$$
{}^{i-1}\mathbf{T}_{i}\left(y_{i}\right)=\begin{bmatrix}\cos\theta_{i} & -\cos\alpha_{i}\sin\theta_{i} & \sin\alpha_{i}\sin\theta_{i} & a_{i}\cos\theta_{i}\\ \sin\theta_{i} & \cos\alpha_{i}\cos\theta_{i} & -\sin\alpha_{i}\cos\theta_{i} & a_{i}\sin\theta_{i}\\ 0 & \sin\alpha_{i} & \cos\alpha_{i} & d_{i}\\ 0 & 0 & 0 & 1\end{bmatrix} \tag{23}
$$

The result of this product is ${}^{0}\mathbf{T}_{7}$, which represents the position and orientation of the end-effector x_7-y_7-z_7 frame relative to the fixed-base x_0-y_0-z_0 frame, as a function of the input coordinates. The forward kinematic mapping required in Eq. (9) can be constructed from Eq. (23), as follows. Output coordinates $\mathbf{z}=\begin{bmatrix}z_1 & z_2 & z_3 & z_4 & z_5 & z_6\end{bmatrix}^{T}$ are defined as position and orientation coordinates of the end-effector relative to the base frame. The position coordinates are extracted from entries (1,4), (2,4), and (3,4) of ${}^{0}\mathbf{T}_{7}$. In the following, the entry of ${}^{0}\mathbf{T}_{7}$ at its i-th row and j-th column is denoted t_{ij}, in which case,

$$
\begin{bmatrix}z_1 & z_2 & z_3\end{bmatrix}^{T}=\begin{bmatrix}t_{14} & t_{24} & t_{34}\end{bmatrix}^{T} \tag{24}
$$

Orientation output coordinates are chosen as three Euler angles; e.g., three successive rotations about moving axes that rotate the base frame until its axes are parallel to those of the end-

effector frame. The first rotation is defined as z_4 about axis X, the second rotation as z_5 about axis Y, and the third rotation as z_6 about axis Z. The rotation angles are obtained from ${}^0\mathbf{T}_7$ as

$$\begin{bmatrix} z_4 & z_5 & z_6 \end{bmatrix}^T = \begin{bmatrix} a & \arcsin(t_{13}) & b \end{bmatrix}^T \tag{25}$$

where arctan2(y,x) is the two-argument inverse tangent that transforms y and x coordinates of a point to its polar angle in the correct quadrant, $a = \arctan2\left(\frac{-t_{23}}{\sqrt{1-t_{13}^2}}, \frac{t_{33}}{\sqrt{1-t_{13}^2}} \right)$, and $b = \arctan2\left(\frac{-t_{12}}{\sqrt{1-t_{13}^2}}, \frac{t_{11}}{\sqrt{1-t_{13}^2}} \right)$. Equations (24) and (25) constitute the input-output equation of Eq. (9) for this manipulator. The self-motion manifold will be obtained for the following end-effector pose, which was obtained by setting $\mathbf{y}$ to the following random value $\bar{\mathbf{y}}^*$, and using Eqs. (24) and (25):

$$\bar{\mathbf{z}} = \begin{bmatrix} 0.7507 \text{ m} \\ -0.4658 \text{ m} \\ 0.6662 \text{ m} \\ 2.8893 \text{ rad} \\ 0.1559 \text{ rad} \\ 0.2839 \text{ rad} \end{bmatrix} \quad \bar{\mathbf{y}}^* = \begin{bmatrix} -0.0007 \\ 0.1533 \\ -0.0770 \\ 0.0371 \\ -0.0226 \\ 0.1117 \\ -0.1089 \end{bmatrix} \text{rad} \tag{26}$$

For 7R redundant manipulators with simplified design, it is possible to construct an analytic parameterization of the inverse kinematic mapping and its self-motion manifold. This is the case for a 7R robot with SRS structure, where the axes of the first three revolute joints intersect at a point, effectively constituting a spherical (S) joint. This is also true for the last three joints of the SRS manipulator. An intermediate revolute joint (R) connects these two spherical joints. The self-motion manifolds of the SRS manipulator can be analytically parameterized by an "arm angle" ψ [10], which is the angle between the plane that contains the arm and some reference plane. As shown therein, the input coordinates of the SRS can be analytically parameterized in terms of ψ, for a desired position and orientation $\bar{\mathbf{z}}$. This is, however, not possible for the 7R arm with generic design.

Another possible method to evaluate the inverse kinematic mapping for a desired $\bar{\mathbf{z}}$ is to choose an input coordinate $\hat{y}_j$ as the independent parameter. This effectively transforms the original redundant manipulator into a nonredundant one, so that the remaining 6 input coordinates $y_i \neq \hat{y}_j$ can be analytically determined as functions of the independent coordinate and $\bar{\mathbf{z}}$. Although this is feasible for simple redundant manipulators [20], for more complex manipulators such as the one studied in this section, this is not practical, or even possible. Since the 7R manipulator studied has a generic design, if any input coordinate is chosen as an independent parameter, the resulting 6R manipulator configuration still has a generic design. It is

known that a generic 6R manipulator admits up to 16 different real solutions for a desired $\bar{\mathbf{z}}$ [21]; i.e., up to sixteen components of the regular configuration space and self-motion manifold. This means that, for a given value of the independent input coordinate $\hat{y}_j$, solving for the remaining six input coordinates requires a costly algebraic elimination procedure to reduce the kinematic equations to a 16-th degree polynomial. This is even worse if the independent input coordinate is varied on a grid to map the self-motion manifold [20], since each node of the grid would require solving this 16-th degree polynomial with updated coefficients.

In summary, there is no practical analytical method to evaluate the inverse kinematic mapping of a general 7R serial manipulator. A formulation such as that presented in Sections 2.1 through 2.6 is required. The self-motion manifold defined by $\bar{\mathbf{z}}$ of Eq. (26) is mapped using the algorithm of Section 2.6. The mapping starts at $\bar{\mathbf{y}}^*$ and travels along a one-dimensional self-motion manifold component until returning again to $\bar{\mathbf{y}}^*$ (considering the wrapping of angles every 2π rad). Computations are carried out using the following algorithmic parameters:

(a) Step h used to map the self-motion manifold: 0.01

(b) Tolerance used in the iterative computation of **h** and **B** according to Appendix A, during mapping of the manifolds, according to Section 2.6: 0.0001.

(c) A reset of v, **U**, **V**, and **B** is performed whenever the distance between the current point $\mathbf{y}^k$ generated on the manifold and the previous one $\mathbf{y}^{k-1}$ exceeds 0.1 rad, i.e.: $\left\|\mathbf{y}^k - \mathbf{y}^{k-1}\right\| > 0.1$.

This is done to prevent the parameterization (v,**V**) from becoming singular, since a sudden change of **y** is a signal that a singularity of the current parameterization is being approached.

When run with MATLAB 2015a on an Intel Core i3-8130U CPU @ 2.20GHz with 8GB RAM, mapping of the manifold takes an average time of 17.7 seconds

Figures 9(a-g) show the evolution of the seven components of $\mathbf{y}$ along the self-motion manifold, whereas Fig. 9(h) shows the projection of the manifold onto the subspace of angles (y_4, y_5, y_6). In Figs. 9(a-g), the horizontal axis represents the index k of each $\mathbf{y}^k$ generated along the manifold. As seen in Fig. 9, all input coordinates except y_2 and y_3 describe closed trajectories. Angles y_2 and y_3 suffer wrapping, such that the difference between their final and initial values is 2π. Accordingly, the initial pose of each body of the robot coincides with its final pose, since adding an integer multiple of 2π to any y_i does not alter the configuration of the robot. Considering wrapping, the self-motion manifold is a closed curve, which starts at $\bar{\mathbf{y}}^*$, travels along the manifold in the direction of the dotted arrow of Fig. 9(h), and ends at $\bar{\mathbf{y}}^*$.

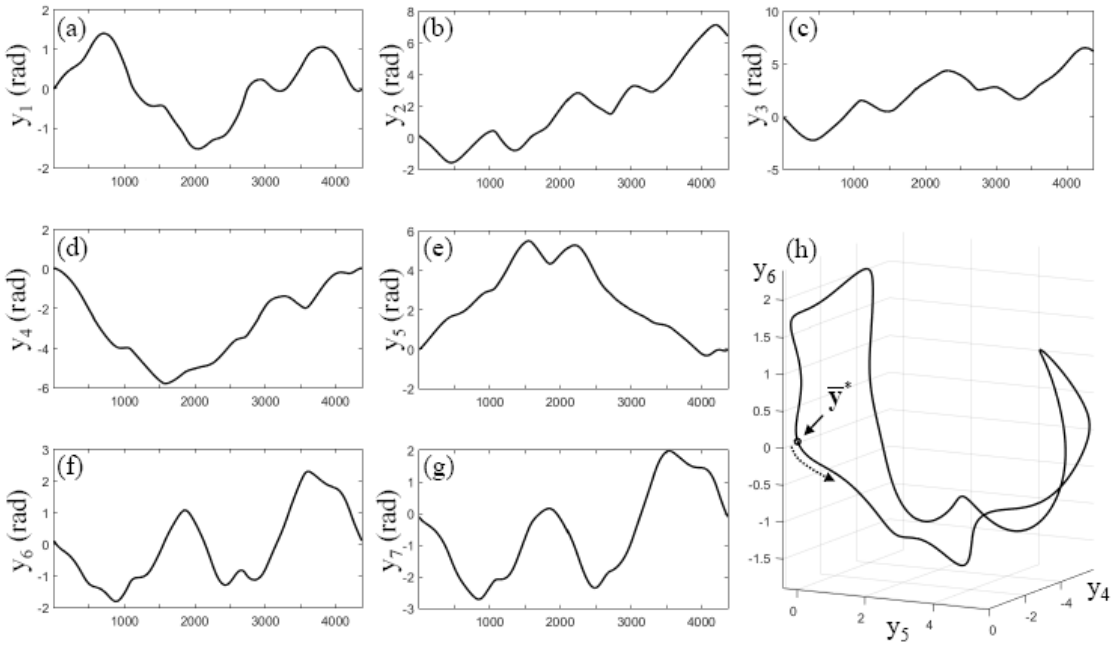

Figure 9 (a-g) Plots of the of y_i Along the Self-Motion Manifold Defined by Eq. (26); Projection of the Self-Motion Manifold on the Subspace of (y_4 y_5 y_6)

3 Kinematically Redundant Compound Manipulators

Consider a manipulator with *input coordinates* $\mathbf{y} \in \mathrm{R}^{\mathrm{n}}$, *generalized coordinates* $\mathbf{q} \in \mathrm{R}^{\mathrm{ngc}}$ of the underlying mechanism, and *output coordinates* $\mathbf{z} \in \mathrm{R}^{\mathrm{m}}$, with m < n. The generalized coordinates are subject to $\mathrm{nhc} = \mathrm{ngc} - \mathrm{n}$ *holonomic constraints*,

$$\mathbf{\Phi}(\mathbf{q}) = \mathbf{0} \tag{27}$$

with $\mathrm{nhc} \times \mathrm{ngc}$ *Jacobian* $\mathbf{\Phi}_{\mathbf{q}}(\mathbf{q}) \equiv \left[\partial \Phi_{\mathrm{i}}(\mathbf{q}) / \mathrm{q}_{\mathrm{j}} \right]$. In neighborhoods of $\mathbf{q}$ at which the constraint Jacobian has full row rank, the mechanism has $\mathrm{n} = \mathrm{ngc} - \mathrm{nhc}$ degrees of freedom. Input and generalized coordinates are required to satisfy n *input equations*,

$$\mathbf{\Psi}(\mathbf{y}, \mathbf{q}) = \mathbf{0} \tag{28}$$

that are intended to determine $\mathbf{y}$ as a function of $\mathbf{q}$ in inverse kinematics. Output and generalized coordinates are required to satisfy m *output equations*,

$$\mathbf{\Gamma}(\mathbf{q}, \mathbf{z}) = \mathbf{0} \tag{29}$$

that are intended to determine $\mathbf{z}$ as a function of $\mathbf{q}$ in forward kinematics. Manipulators with this structure are called *compound kinematically redundant manipulators*.

3.1 Compound Manipulator Configuration Space

With *manipulator coordinates* $\mathbf{x} = \left[\mathbf{y}^{\mathrm{T}} \quad \mathbf{q}^{\mathrm{T}} \quad \mathbf{z}^{\mathrm{T}} \right]^{\mathrm{T}} \in \mathrm{R}^{\mathrm{n+ngc+m}}$, the *compound manipulator configuration space* is defined as $\mathrm{X}^{\mathrm{c}} = \left\{ \mathbf{x} \in \mathrm{R}^{\mathrm{n+ngc+m}} : \mathbf{\Phi}(\mathbf{q}) = \mathbf{0}, \mathbf{\Psi}(\mathbf{y}, \mathbf{q}) = \mathbf{0}, \text{ and } \mathbf{\Gamma}(\mathbf{q}, \mathbf{z}) = \mathbf{0} \right\}$. While this space characterizes the geometry of the manipulator, it contains singular configurations that preclude desirable manipulator input and output relations.

The combined equations

$$\mathbf{\Omega}(\mathbf{y},\mathbf{q}) \equiv \begin{bmatrix} \mathbf{\Phi}(\mathbf{q}) \\ \mathbf{\Psi}(\mathbf{y},\mathbf{q}) \end{bmatrix} = \mathbf{0} \tag{30}$$

comprise a system of $\mathrm{nhc} + \mathrm{n} = \mathrm{ngc}$ equations that are intended to determine $\mathbf{q}$ as a function of $\mathbf{y}$ in forward kinematics. A sufficient condition that this is possible, in a neighborhood of a configuration $\bar{\mathbf{x}} \in \mathrm{X}^{\mathrm{c}}$, is

$$\left|\mathbf{\Omega}_{\mathbf{q}}(\bar{\mathbf{y}},\bar{\mathbf{q}})\right| = \left\| \begin{bmatrix} \mathbf{\Phi}_{\mathbf{q}}(\bar{\mathbf{q}}) \\ \mathbf{\Psi}_{\mathbf{q}}(\bar{\mathbf{y}},\bar{\mathbf{q}}) \end{bmatrix} \right\| \neq \mathbf{0} \tag{31}$$

In this case, the implicit function theorem [15] implies there is a unique solution of Eq. (30),

$$\mathbf{q} = \mathbf{f}(\mathbf{y}) \tag{32}$$

in a neighborhood of $\bar{\mathbf{y}}$. The m output equations of Eq. (29) are intended to determine $\mathbf{z} \in \mathrm{R}^{\mathrm{m}}$ as a function of $\mathbf{q}$ in forward kinematics. A sufficient condition for this is

$$\left|\mathbf{\Gamma}_{\mathbf{z}}(\bar{\mathbf{q}},\bar{\mathbf{z}})\right| \neq 0 \tag{33}$$

which assures existence of a unique solution,

$$\mathbf{z} = \mathbf{e}(\mathbf{q}) \tag{34}$$

in a neighborhood of $\bar{\mathbf{q}}$. Under the foregoing sufficiency conditions, Eqs. (32) and (34) yield the *forward kinematic mapping* that is key to control of the manipulator,

$$\mathbf{z} = \mathbf{e}(\mathbf{f}(\mathbf{y})) \equiv \mathbf{G}(\mathbf{y}) \tag{35}$$

Since the dimension m of $\mathbf{z}$ is less than the dimension n of $\mathbf{y}$, there is no prospect for a single valued inverse kinematic mapping from $\mathbf{z}$ to $\mathbf{y}$ that corresponds to Eq. (35). In fact, the combined conditions of Eqs. (27) and (29),

$$\mathbf{\Lambda}(\mathbf{q},\mathbf{z}) \equiv \begin{bmatrix} \mathbf{\Phi}(\mathbf{q}) \\ \mathbf{\Gamma}(\mathbf{q},\mathbf{z}) \end{bmatrix} = \mathbf{0} \tag{36}$$

comprise $\mathrm{nhc} + \mathrm{m} = \mathrm{ngc} - (\mathrm{n} - \mathrm{m}) < \mathrm{ngc}$ equations in ngc generalized coordinates $\mathbf{q}$. There cannot exist, therefore, a unique solution of Eq. (36) for $\mathbf{q}$ as a function of $\mathbf{z}$. If the Jacobian $\mathbf{\Lambda}_{\mathbf{q}}(\bar{\mathbf{q}},\bar{\mathbf{z}})$ has full row rank $\mathrm{ngc} - (\mathrm{n} - \mathrm{m})$ for $\bar{\mathbf{x}} \in \tilde{\mathrm{X}}^{\mathrm{c}}$, Eq. (36) has an $(\mathrm{ngc} - (\mathrm{n} - \mathrm{m})) \times (\mathrm{ngc} - (\mathrm{n} - \mathrm{m}))$ nonsingular submatrix. The implicit function theorem then implies that the associated $\mathrm{ngc} - (\mathrm{n} - \mathrm{m})$ elements of $\mathbf{q} \in \mathrm{R}^{\mathrm{ngc}}$ can be determined by Eq. (36) as functions of $\mathbf{z}$ and the remaining $\mathrm{n} - \mathrm{m}$ elements of $\mathbf{q}$; i.e., an $\mathrm{n} - \mathrm{m}$ parameter family of solutions of Eq. (36) for $\mathbf{z}$, in a neighborhood of $\bar{\mathbf{z}}$. A sufficient condition that the n input equations of Eq. (28) determine $\mathbf{y} \in \mathrm{R}^{\mathrm{n}}$ as a function of $\mathbf{q}$ in inverse kinematics is

$$\left|\mathbf{\Psi}_{\mathrm{y}}(\bar{\mathbf{y}},\bar{\mathbf{q}})\right| \neq \mathrm{o} \tag{37}$$

which assures existence of a unique solution of Eq. (28), in a neighborhood of $\bar{\mathbf{q}}$,

$$\mathbf{y} = \mathbf{g}(\mathbf{q}) \tag{38}$$

Thus, the n – m parameter inverse kinematic mapping from **z** to **q** defined by Eq. (36) yields an n – m parameter inverse mapping from **z** to **y**, using Eq. (38).

3.2 Regular Compound Manipulator Configuration Space

To assure existence of the foregoing manipulator properties and to avoid singular configurations that occur in $\mathrm{X}^{\mathbf{c}}$, the *compound manipulator regular configuration space* is defined as $\tilde{\mathrm{X}}^{\mathbf{c}} = \left\{ \begin{array}{l} \mathbf{x} \in \mathrm{X}^{\mathbf{c}} : \left|\boldsymbol{\Omega}_{\mathbf{q}}(\mathbf{y},\mathbf{q})\right| \neq 0, \left|\boldsymbol{\Psi}_{\mathbf{y}}(\mathbf{y},\mathbf{q})\right| \neq 0, \\ \qquad \left|\boldsymbol{\Lambda}_{\mathbf{q}}(\mathbf{q},\mathbf{z})\boldsymbol{\Lambda}_{\mathbf{q}}^{\mathrm{T}}(\mathbf{q},\mathbf{z})\right| \neq 0, \ \textbf{and} \ \left|\boldsymbol{\Gamma}_{\mathbf{z}}(\mathbf{q},\mathbf{z})\right| \neq 0 \end{array} \right\}$ Since this is an open subset of $\mathrm{X}^{\mathbf{c}}$ in the relative topology of $\mathrm{X}^{\mathrm{c}} \subset \mathrm{R}^{\mathrm{n+ngc+m}}$, it is comprised of a collection of *disjoint, maximal, path connected, singularity free components* $\tilde{\mathrm{X}}_{\mathrm{i}}^{\mathbf{c}}$ [16]. Further, $\tilde{\mathrm{X}}_{\mathrm{i}}^{\mathbf{c}} \cap \tilde{\mathrm{X}}_{\mathrm{j}}^{\mathbf{c}} = \varphi$ if $\mathrm{i} \neq \mathrm{j}$ and $\cup_{\mathrm{i}} \tilde{\mathrm{X}}_{\mathrm{i}}^{\mathbf{c}} = \tilde{\mathrm{X}}^{\mathbf{c}}$. For $\bar{\mathbf{x}} \in \tilde{\mathrm{X}}^{\mathbf{c}}$, the functions $\mathbf{f}(\mathbf{y})$ and $\mathbf{e}(\mathbf{q})$ of Eqs. (32) and (34) are continuously differentiable and $\boldsymbol{\psi}(\mathbf{y}) = \left[\mathbf{y}^{\mathrm{T}} \quad \mathbf{f}^{\mathrm{T}}(\mathbf{y}) \quad \mathbf{e}^{\mathrm{T}}(\mathbf{f}(\mathbf{y}))\right]^{\mathrm{T}} = \mathbf{x} \in \tilde{\mathrm{X}}^{\mathbf{c}}$ is a differentiable mapping from open subsets of R^{n} onto open subsets of $\tilde{\mathrm{X}}^{\mathbf{c}}$, with inverse mapping $\boldsymbol{\phi}(\mathbf{x}) = \mathbf{y}$. As shown in [1], $\tilde{\mathrm{X}}^{\mathbf{c}}$ and its components are *differentiable manifolds*, parameterized by $\mathbf{y} \in \mathrm{R}^{\mathrm{n}}$.

3.3 Compound Manipulator Inverse Kinematic Configuration Mapping

While regularity properties of functions involved in the definition of $\tilde{\mathrm{X}}^{\mathbf{c}}$ assure local existence of a single valued forward kinematic mapping of Eq. (35), they do not assure existence of a single valued inverse kinematic mapping from **z** to **y**. In fact, since $\mathbf{y} \in \mathrm{R}^{\mathrm{n}}$, $\mathbf{z} \in \mathrm{R}^{\mathrm{m}}$, and n > m, such an inverse mapping is necessarily *set-valued*; i.e., from Eq. (35)

$$\mathbf{G}^{-1}(\mathbf{z}) = \left\{\mathbf{y} : \mathbf{z} = \mathbf{G}(\mathbf{y})\right\} \subset \mathrm{R}^{\mathrm{n}} \tag{39}$$

The first step in characterizing the set-valued inverse mapping of Eq. (39) is to find all **q** that satisfy Eq. (36) for a given **z**. Since this is a system of $\mathrm{nhc} + \mathrm{m}$ equations in ngc variables and $\boldsymbol{\Lambda}_{\mathbf{q}}(\mathbf{q},\mathbf{z})$ has row rank $\mathrm{ngc} - (\mathrm{n} - \mathrm{m})$ in $\tilde{\mathrm{X}}^{\mathbf{c}}$, there is an $\mathrm{n} - \mathrm{m}$ parameter family of solutions of Eq. (36). To construct this family in a neighborhood of $\bar{\mathbf{x}} \in \tilde{\mathrm{X}}^{\mathbf{c}}$, define

$$\mathbf{U} = \boldsymbol{\Lambda}_{\mathbf{q}}^{\mathrm{T}}(\bar{\mathbf{q}}, \bar{\mathbf{z}}) \tag{40}$$

that has column rank $\mathrm{ngc} - (\mathrm{n} - \mathrm{m})$, and use *singular value decomposition*

$$\boldsymbol{\Lambda}_{\mathbf{q}}(\bar{\mathbf{q}}, \bar{\mathbf{z}})\mathbf{V} = \mathbf{0} \quad \mathbf{V}^{\mathrm{T}}\mathbf{V} = \mathbf{I} \tag{41}$$

to obtain **V** with column rank $\mathrm{n} - \mathrm{m}$ [17]. Since the columns of **V** and **U** span $\mathrm{R}^{\mathrm{ngc}}$, any solution **q** of Eq. (36) may be represented as

$$\mathbf{q} = \bar{\mathbf{q}} + \mathbf{V}\mathbf{v} - \mathbf{U}\mathbf{u} \tag{42}$$

where $\mathbf{v} \in \mathrm{R}^{\mathrm{n-m}}$ and $\mathbf{u} \in \mathrm{R}^{\mathrm{ngc-(n-m)}}$. Note that at $\mathbf{q} = \bar{\mathbf{q}}$, $\mathbf{v} = \bar{\mathbf{v}} = \mathbf{0}$ and $\mathbf{u} = \bar{\mathbf{u}} = \mathbf{0}$. In order for **q** of Eq. (42) to satisfy Eq. (36), for given values of **v** and **z**, **u** must satisfy

$$\boldsymbol{\Lambda}(\bar{\mathbf{q}} + \mathbf{V}\mathbf{v} - \mathbf{U}\mathbf{u}, \mathbf{z}) = \mathbf{0} \tag{43}$$

The Jacobian of the left side of this equation with respect to **u**, evaluated at $\bar{\mathbf{x}}$, is $\boldsymbol{\Lambda}(\hat{\bar{\mathbf{q}}} + \mathbf{V}\hat{\mathbf{v}} - \mathbf{U}\mathbf{u}, \hat{\mathbf{z}})_{\mathbf{u}} = -\boldsymbol{\Lambda}_{\mathbf{q}}(\bar{\mathbf{q}}, \bar{\mathbf{z}})\mathbf{U} = -\mathbf{U}^{\mathrm{T}}\mathbf{U}$, which is nonsingular. Therefore, there exists a unique differentiable solution $\mathbf{u} = \mathbf{h}(\mathbf{v}, \mathbf{z})$ of Eq. (43), for all $(\mathbf{v}, \mathbf{z})$ in a neighborhood of $(\mathbf{0}, \bar{\mathbf{z}})$. The solution of Eq. (36) for **q** is thus

$$\mathbf{q}(\mathbf{v}, \mathbf{z}) = \bar{\mathbf{q}} + \mathbf{V}\mathbf{v} - \mathbf{U}\mathbf{h}(\mathbf{v}, \mathbf{z}) \tag{44}$$

for any $\mathbf{v} \in \mathrm{R}^{n-m}$ in a neighborhood of **0** and **z** in a neighborhood of $\bar{\mathbf{z}}$. Using Eq. (38),

$$\mathbf{y}(\mathbf{v}, \mathbf{z}) = \mathbf{g}(\bar{\mathbf{q}} + \mathbf{V}\mathbf{v} - \mathbf{U}\mathbf{h}(\mathbf{v}, \mathbf{z})) \tag{45}$$

for any $\mathbf{v} \in \mathrm{R}^{n-m}$ in a neighborhood of **0** and **z** in a neighborhood of $\bar{\mathbf{z}}$.

3.4 Parameterization of the Regular Compound Manipulator Configuration Space

Equation (45) provides a continuously differentiable parameterization of $\tilde{\mathrm{X}}^{\mathbf{s}}$ on a neighborhood N of $(\mathbf{0}, \bar{\mathbf{z}})$; i.e.,

$$\tilde{\mathrm{X}}^{\mathbf{c}}_{\mathrm{N}} = \left\{ \begin{array}{l} \mathbf{x} \in \mathrm{X}^{\mathbf{c}} : \mathbf{q} = \bar{\mathbf{q}} + \mathbf{V}\mathbf{v} - \mathbf{U}\mathbf{h}(\mathbf{v}, \mathbf{z}), \mathbf{y} = \mathbf{g}(\mathbf{q}), \\ \qquad \text{for all } \mathbf{v} \text{ in a neighborhood of } \mathbf{0} \\ \qquad \text{and } \mathbf{z} \text{ in a neighborhood of } \bar{\mathbf{z}} \end{array} \right\} \tag{46}$$

Neighborhoods assured by the implicit function theorem and the mappings of Eqs. (44) and (45) define a *chart* on $\tilde{\mathrm{X}}^{\mathbf{c}}$. Creating a family of such charts that cover $\tilde{\mathrm{X}}^{\mathbf{c}}$ provides an *atlas* that defines $\tilde{\mathrm{X}}^{\mathbf{c}}$ as a *differentiable manifold* with disjoint, maximal, path connected, singularity free components $\tilde{\mathrm{X}}^{\mathbf{c}}_{\mathrm{i}}$ [14]. The basis for this extension of local charts to the global manifold $\tilde{\mathrm{X}}^{\mathbf{c}}$ is as outlined in Section 2.4.

For use in manipulator kinematic analysis and control, partial derivatives of $\mathbf{h}(\mathbf{v}, \mathbf{z})$, $\mathbf{q}(\mathbf{v}, \mathbf{z})$, and $\mathbf{y}(\mathbf{v}, \mathbf{z})$ with respect to **v** and **z** are needed. To obtain $\mathbf{h}_{\mathbf{v}}(\mathbf{v}, \mathbf{z})$ and $\mathbf{h}_{\mathbf{z}}(\mathbf{v}, \mathbf{z})$, the partial derivatives of Eq. (43) with respect to **v** and **z**, evaluated at $\mathbf{u} = \mathbf{h}(\mathbf{v}, \mathbf{z})$, are

$$\begin{aligned} \boldsymbol{\Lambda}_{\mathbf{q}}\left(\mathbf{V} - \mathbf{U}\mathbf{h}_{\mathbf{v}}\right) &= \mathbf{0} \\ \boldsymbol{\Lambda}_{\mathbf{q}}\left(-\mathbf{U}\mathbf{h}_{\mathbf{z}}\right) + \boldsymbol{\Lambda}_{\mathbf{z}} &= \mathbf{0} \end{aligned} \tag{47}$$

Since $\boldsymbol{\Lambda}_{\mathbf{q}}\mathbf{U} = \mathbf{U}^{\mathrm{T}}\mathbf{U}$ is nonsingular at $\bar{\mathbf{x}}$ and $\boldsymbol{\Lambda}_{\mathbf{q}}(\mathbf{q}, \mathbf{z})$ is a differentiable function of **q** and **z**,

$$\mathbf{B}(\mathbf{v}, \mathbf{z}) \equiv \left(\boldsymbol{\Lambda}_{\mathbf{q}}(\mathbf{q}(\mathbf{v}, \mathbf{z}), \mathbf{z})\mathbf{U}\right)^{-1} \tag{48}$$

is nonsingular and differentiable in a neighborhood of $\bar{\mathbf{x}}$. Using Eq. (48) in Eqs. (47),

$$\begin{aligned} \mathbf{h}_{\mathbf{v}}(\mathbf{v}, \mathbf{z}) &= \mathbf{B}(\mathbf{v}, \mathbf{z})\boldsymbol{\Lambda}_{\mathbf{q}}(\mathbf{q}(\mathbf{v}, \mathbf{z}), \mathbf{z})\mathbf{V} \\ \mathbf{h}_{\mathbf{z}}(\mathbf{v}, \mathbf{z}) &= \mathbf{B}(\mathbf{v}, \mathbf{z})\boldsymbol{\Lambda}_{\mathbf{z}}(\mathbf{q}(\mathbf{v}, \mathbf{z}), \mathbf{z}) \end{aligned} \tag{49}$$

Using these results with Eq. (44),

$$\begin{aligned} \mathbf{q}_{\mathbf{v}}(\mathbf{v}, \mathbf{z}) &= \mathbf{V} - \mathbf{U}\mathbf{B}(\mathbf{v}, \mathbf{z})\boldsymbol{\Lambda}_{\mathbf{q}}(\mathbf{q}(\mathbf{v}, \mathbf{z}), \mathbf{z})\mathbf{V} \\ \mathbf{q}_{\mathbf{z}}(\mathbf{v}, \mathbf{z}) &= -\mathbf{U}\mathbf{B}(\mathbf{v}, \mathbf{z})\boldsymbol{\Lambda}_{\mathbf{z}}(\mathbf{q}(\mathbf{v}, \mathbf{z}), \mathbf{z}) \end{aligned} \tag{50}$$

Likewise, with Eq. (45), $\mathbf{y}_{\mathbf{v}}(\mathbf{v},\mathbf{z}) = \mathbf{g}'(\mathbf{q}(\mathbf{v},\mathbf{z}))\mathbf{q}_{\mathbf{v}}(\mathbf{v},\mathbf{z})$ and $\mathbf{y}_{\mathbf{z}}(\mathbf{v},\mathbf{z}) = \mathbf{g}'(\mathbf{q}(\mathbf{v},\mathbf{z}))\mathbf{q}_{\mathbf{z}}(\mathbf{v},\mathbf{z})$. Since $\boldsymbol{\Psi}(\mathbf{g}(\mathbf{q}),\mathbf{q}) = \mathbf{0}$ is an identity in $\mathbf{q}$, $\boldsymbol{\Psi}_{\mathbf{y}}(\mathbf{g}(\mathbf{q}),\mathbf{q})\mathbf{g}'(\mathbf{q}) + \boldsymbol{\Psi}_{\mathbf{q}}(\mathbf{g}(\mathbf{q}),\mathbf{q}) = \mathbf{0}$ in $\tilde{\mathrm{X}}^{\mathbf{c}}$, where $\left|\boldsymbol{\Psi}_{\mathbf{y}}(\mathbf{g}(\mathbf{q}),\mathbf{q})\right| \neq 0$. Thus,

$$\mathbf{g}'(\mathbf{q}) = -\boldsymbol{\Psi}_{\mathbf{y}}^{-1}(\mathbf{g}(\mathbf{q}),\mathbf{q})\boldsymbol{\Psi}_{\mathbf{q}}(\mathbf{g}(\mathbf{q}),\mathbf{q}) \tag{51}$$

and, using Eq. (50),

$$\begin{aligned}\mathbf{y}_{\mathbf{v}}(\mathbf{v},\mathbf{z}) &= \mathbf{g}'(\bar{\mathbf{q}} + \mathbf{V}\mathbf{v} - \mathbf{U}\mathbf{h}(\mathbf{v},\mathbf{z}))\left(\mathbf{V} - \mathbf{U}\mathbf{B}(\mathbf{v},\mathbf{z})\boldsymbol{\Lambda}_{\mathbf{q}}(\mathbf{q}(\mathbf{v},\mathbf{z}),\mathbf{z})\mathbf{V}\right)\\ \mathbf{y}_{\mathbf{z}}(\mathbf{v},\mathbf{z}) &= -\mathbf{g}'(\bar{\mathbf{q}} + \mathbf{V}\mathbf{v} - \mathbf{U}\mathbf{h}(\mathbf{v},\mathbf{z}))\mathbf{U}\mathbf{B}(\mathbf{v},\mathbf{z})\boldsymbol{\Lambda}_{\mathbf{z}}(\mathbf{q}(\mathbf{v},\mathbf{z}),\mathbf{z})\end{aligned} \tag{52}$$

The derivatives of Eqs. (49), (50) and (52) enable redundant compound manipulator applications such as obstacle and singularity avoidance and dynamic performance optimization.

3.5 The Compound Manipulator Self-Motion Manifold

For fixed $\mathbf{z} = \bar{\mathbf{z}}$ with $\bar{\mathbf{x}} \in \tilde{\mathrm{X}}_{\mathrm{i}}^{\mathbf{c}}$, the mapping of Eq. (45) is

$$\mathbf{y}(\mathbf{v},\bar{\mathbf{z}}) = \mathbf{g}(\bar{\mathbf{q}} + \mathbf{V}\mathbf{v} - \mathbf{U}\mathbf{h}(\mathbf{v},\bar{\mathbf{z}})) \tag{53}$$

for all $\mathbf{v}$ in a neighborhood of $\mathbf{0}$. This yields sets of inputs

$$\mathbf{Y}_{\mathrm{N}}^{\mathbf{c}}(\bar{\mathbf{z}}) = \left\{\begin{array}{l}\mathbf{y} : \mathbf{y} = \mathbf{g}(\bar{\mathbf{q}} + \mathbf{V}\mathbf{v} - \mathbf{U}\mathbf{h}(\mathbf{v},\bar{\mathbf{z}})),\\ \qquad \text{for all } \mathbf{v} \in \mathrm{R}^{\mathrm{n-m}} \text{ in a neighborhood N of } \mathbf{0}\end{array}\right\}$$

whose union $\mathbf{Y}^{\mathbf{c}}(\bar{\mathbf{z}})$ is a differentiable manifold in input space. This manifold is called the *self-motion manifold*, since it is a set of inputs, all of which have forward kinematic mappings onto the same output $\bar{\mathbf{z}}$. The inverse kinematic mapping of Eq. (53) is a parameterization of $\mathbf{Y}^{\mathbf{c}}(\bar{\mathbf{z}})$. Thus, $\mathbf{Y}^{\mathbf{c}}(\bar{\mathbf{z}})$ is a set of inputs that all yield $\bar{\mathbf{z}}$, some of which may have attractive properties such as avoiding obstacles and singularities. As with all differentiable manifolds, $\mathbf{Y}^{\mathbf{c}}(\bar{\mathbf{z}})$ may be partitioned into maximal disjoint submanifolds $\mathbf{Y}_{\mathrm{i}}^{\mathbf{c}}(\bar{\mathbf{z}})$; i.e., in general, $\mathbf{Y}^{\mathbf{c}}(\bar{\mathbf{z}})$ is not a connected set.

If $\bar{\mathbf{z}}_{\mathrm{i}}$ and $\bar{\mathbf{z}}_{\mathrm{j}}$ are adjacent outputs in a neighborhood of $\bar{\mathbf{z}}$, one may select vastly different $\bar{\mathbf{y}}_{\mathrm{i}} \in \mathbf{Y}^{\mathbf{c}}(\bar{\mathbf{z}}_{\mathrm{i}})$ and $\bar{\mathbf{y}}_{\mathrm{j}} \in \mathbf{Y}^{\mathbf{c}}(\bar{\mathbf{z}}_{\mathrm{j}})$, so the resulting $\bar{\mathbf{x}}_{\mathrm{i}}$ and $\bar{\mathbf{x}}_{\mathrm{j}}$ are distinctly different in $\tilde{\mathrm{X}}^{\mathbf{c}}$. If one wishes to maintain manipulator configuration continuity in $\tilde{\mathrm{X}}^{\mathbf{c}}$, large uncorrelated excursions in $\mathbf{Y}^{\mathbf{c}}(\bar{\mathbf{z}})$, with $\mathbf{z} = \bar{\mathbf{z}}$ fixed, must be avoided. In short, the manipulator regular configuration manifold $\tilde{\mathrm{X}}^{\mathbf{c}}$ and the self-motion manifold $\mathbf{Y}^{\mathbf{c}}(\bar{\mathbf{z}})$ are fundamentally different.

3.6 Mapping One-Dimensional Compound Manipulator Self-Motion Manifold Components

A self-motion manifold component $\mathbf{Y}_{\mathrm{i}}^{\mathbf{c}}(\bar{\mathbf{z}})$ with $\mathrm{n} - \mathrm{m} = 1$ is to be mapped, beginning at a configuration $\bar{\mathbf{x}} = \left[\bar{\mathbf{y}}^{\mathrm{T}} \quad \bar{\mathbf{q}}^{\mathrm{T}} \quad \bar{\mathbf{z}}^{\mathrm{T}}\right]^{\mathrm{T}} \in \tilde{\mathrm{X}}$. The output $\bar{\mathbf{z}}$ is held fixed during the process of mapping $\mathbf{Y}_{\mathrm{i}}^{\mathbf{c}}(\bar{\mathbf{z}})$, as follows:

(1) At $\mathbf{y} = \bar{\mathbf{y}}$, $v^0 = 0$, use Eqs. (40) and (41) to evaluate **U** and **V** and evaluate $\mathbf{B}^0 = \mathbf{B}(0, \bar{\mathbf{z}}) = \left(\mathbf{U}^T\mathbf{U}\right)^{-1}$.

(2) For a small step h > 0 in v, set $v^1 = h$ and obtain $\mathbf{h}(\mathbf{v}^1, \bar{\mathbf{z}})$, using the iterative process of Eq. (62) with $\mathbf{B} = \mathbf{B}^0$ for $\mathbf{u}^1 = \mathbf{h}(\mathbf{v}^1, \bar{\mathbf{z}})$.

(3) Evaluate generalized coordinates $\mathbf{q}^1(\mathbf{v}, \bar{\mathbf{z}}) = \bar{\mathbf{q}} + \mathbf{V}v^1 - \mathbf{U}\mathbf{h}(\mathbf{v}^1, \bar{\mathbf{z}})$ in Eq. (44) and obtain $\mathbf{y}^1$ by solving $\boldsymbol{\Psi}(\mathbf{y}, \mathbf{q}^1) = \mathbf{0}$ of Eq. (28), using Newton-Raphson iteration, beginning with estimate $\mathbf{y}^{(1)} = \bar{\mathbf{y}}$.

(4) Use the iterative process of Eq. (61) to evaluate $\mathbf{B}^1$.

(5) At $v^k = kh$, $k = 2,\ldots$, evaluate $\mathbf{h}(\mathbf{v}^k, \bar{\mathbf{z}})$ as $\mathbf{u}^k = \mathbf{h}(\mathbf{v}^k, \bar{\mathbf{z}})$ from Eq. (62) with $\mathbf{B} = \mathbf{B}^{k-1}$ and $\mathbf{q}^k(\mathbf{v}^k, \bar{\mathbf{z}}) = \bar{\mathbf{q}} + \mathbf{V}v^k - \mathbf{U}\mathbf{h}(v^k, \bar{\mathbf{z}})$ from Eq. (44).

(6) Evaluate $\mathbf{y}^k$ by iterative solution of $\boldsymbol{\Psi}(\mathbf{y}, \mathbf{q}^k) = \mathbf{0}$ in Eq. (28), beginning with estimate $\mathbf{y}^{(k)} = \mathbf{y}^{k-1}$, and evaluate $\mathbf{B}^k$ using the iterative process of Eq. (61).

(7) Confirm $\left|\boldsymbol{\Lambda}_{\mathbf{q}}(\mathbf{q}^k, \bar{\mathbf{z}})\boldsymbol{\Lambda}_{\mathbf{q}}^T(\mathbf{q}^k, \bar{\mathbf{z}})\right|$ to be positive to assure $\mathbf{y}^k \in \mathbf{Y}_i^{\mathbf{c}}(\bar{\mathbf{z}})$.

(8) Confirm that $\left|\boldsymbol{\Lambda}_{\mathbf{q}}(\mathbf{y}^k, \bar{\mathbf{z}})\mathbf{U}\right|$ has the same sign throughout the mapping process.

(9) If the condition number [17] of $\boldsymbol{\Lambda}_{\mathbf{q}}(\mathbf{y}^k, \bar{\mathbf{z}})\mathbf{U}$ is within tolerance, continue the mapping process.

(10) Otherwise, redefine $\bar{\mathbf{y}} = \mathbf{y}^k$ and $\bar{\mathbf{q}} = \mathbf{q}^k$, retain $\mathbf{z} = \bar{\mathbf{z}}$, use Eqs. (40) and (41) to evaluate new matrices **U** and **V**, reset $v^0 = 0$, evaluate $\mathbf{B}^0 = \left(\mathbf{U}^T\mathbf{U}\right)^{-1}$, index $v^k = kh$, and continue the mapping process.

This process is as outlined on charts of the differentiable manifold in Section 2.4 and shown schematically in Fig. 4.

3.7 Model Kinematically Redundant Compound Manipulator Kinematics

The two-bar model manipulator shown in Fig. 10 has a pin at the left end of body 2 that slides in a slot in body 1. The output point P is 2 m to the right of the origin of the body 1 reference frame. The model has 3 input coordinates, 5 generalized coordinates, and 2 output coordinates. The condition that the pin on body 2 slides in the slot in body 1 is the holonomic constraint

$$\begin{aligned}\boldsymbol{\Phi}(\mathbf{q}) &= q_1\mathbf{u}_y + q_5\mathbf{A}(q_2)\mathbf{u}_x - \left(q_3\mathbf{u}_x - \mathbf{A}(q_4)\mathbf{u}_x\right) \\ &= \begin{bmatrix} q_5\cos q_2 - q_3 + \cos q_4 \\ q_1 + q_5\sin q_2 + \sin q_4 \end{bmatrix} = \mathbf{0}\end{aligned} \tag{54}$$

Input and output equations are

$$\boldsymbol{\Psi}(\mathbf{y}, \mathbf{q}) = \begin{bmatrix} q_3 - y_1 & q_1 - y_2 & q_5 - y_3 \end{bmatrix}^T = \mathbf{0} \tag{55}$$

$$\boldsymbol{\Gamma}(\mathbf{q}, \mathbf{z}) = \begin{bmatrix} 2\cos q_2 - z_1 & q_1 + 2\sin q_2 - z_2 \end{bmatrix}^T = \mathbf{0} \tag{56}$$

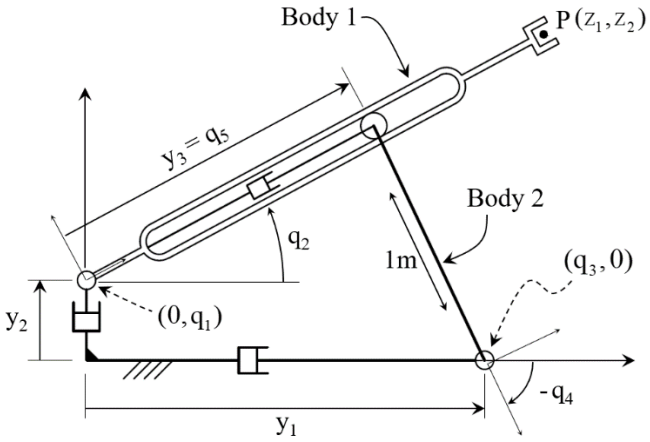

Figure 10 Model Compound Manipulator

Jacobians $\boldsymbol{\Psi}_{\mathbf{y}}(\mathbf{y},\mathbf{q})$ and $\boldsymbol{\Gamma}_{\mathbf{z}}(\mathbf{q},\mathbf{z})$ are nonsingular, leading to the solutions

$$\begin{aligned}\mathbf{y} &= \begin{bmatrix} q_3 & q_1 & q_5 \end{bmatrix}^{\mathrm{T}} \\ \mathbf{z} &= \begin{bmatrix} 2\cos q_2 & q_1 + 2\sin q_2 \end{bmatrix}^{\mathrm{T}}\end{aligned} \tag{57}$$

The composite Jacobian

$$\begin{aligned}\boldsymbol{\Omega}_{\mathbf{q}}(\mathbf{y},\mathbf{q}) &= \begin{bmatrix} \boldsymbol{\Phi}_{\mathbf{q}}(\mathbf{q}) \\ \boldsymbol{\Psi}_{\mathbf{q}}(\mathbf{y},\mathbf{q}) \end{bmatrix} \\ &= \begin{bmatrix} 0 & -q_5\sin q_2 & -1 & -\sin q_4 & \cos q_2 \\ 1 & q_5\cos q_2 & 0 & \cos q_4 & \sin q_2 \\ 0 & 0 & 1 & 0 & 0 \\ 1 & 0 & 0 & 0 & 0 \\ 0 & 0 & 0 & 0 & 1 \end{bmatrix}\end{aligned} \tag{58}$$

has determinant $\left|\boldsymbol{\Omega}_{\mathbf{q}}(\mathbf{y},\mathbf{q})\right| = q_5\sin(q_4 - q_2)$. Thus, as long as $q_5 = y_3 \neq 0$ and the bars are not colinear; i.e., $\sin(q_4 - q_2) \neq 0,$ there is a unique solution $\mathbf{q} = \mathbf{f}(\mathbf{y})$ of $\boldsymbol{\Omega}(\mathbf{y},\mathbf{q}) = \mathbf{0}$ in each component of $\tilde{\mathrm{X}}^{\mathbf{c}}$. The composite 4×5 Jacobian matrix

$$\begin{aligned}\boldsymbol{\Lambda}_{\mathbf{q}}(\mathbf{q},\mathbf{z}) &= \begin{bmatrix} \boldsymbol{\Phi}_{\mathbf{q}}(\mathbf{q}) \\ \boldsymbol{\Gamma}_{\mathbf{q}}(\mathbf{q},\mathbf{z}) \end{bmatrix} \\ &= \begin{bmatrix} 0 & -q_5\sin q_2 & -1 & -\sin q_4 & \cos q_4 \\ 1 & q_5\cos q_2 & 0 & \cos q_4 & \sin q_4 \\ 0 & -2\sin q_2 & 0 & 0 & 0 \\ 1 & 2\cos q_2 & 0 & 0 & 0 \end{bmatrix}\end{aligned} \tag{59}$$

should have full row rank. Setting $\boldsymbol{\Lambda}_{\mathbf{q}}^{\mathrm{T}}(\mathbf{q},\mathbf{z})\mathbf{a} = \mathbf{0}$ leads to the following equations: $a_2 + a_4 = 0,$ $-q_5\sin q_2 a_1 + q_5\cos q_2 a_2 - 2\sin q_2 a_3 + 2\cos q_2 a_4 = 0,$ $a_1 = 0,$ $-\sin q_4 a_1 + \cos q_4 a_2 = 0,$ and

$\cos q_4 a_1 + \sin q_4 a_2 = 0$. Thus, $a_1 = 0,\ \cos q_4 a_2 = 0 = \sin q_4 a_2 \Rightarrow a_2 = 0,\ a_4 = 0,$ and $-2\sin q_2 a_3 = 0 \Rightarrow a_3 = 0$ if $\sin q_2 \neq 0$. This shows that the composite Jacobian $\mathbf{\Lambda_q(q,z)}$ has full row rank if $\sin q_2 \neq 0$. If $\sin q_2 = 0$, bar 1 is horizontal and $\mathbf{\Lambda_q(q,z)}$ fails to have full row rank. With bar 1 horizontal and to the right of the vertical axis, if $\delta z_1 > 0$ there is no solution for $\mathbf{q}$ and if $\delta z_1 < 0$ there are two distinctly different solutions. This gives insight into the physical significance of the singularity $\sin q_2 = 0$.

The configuration space for this manipulator is $X^c = \{\mathbf{x} \in R^{10} : \mathbf{\Phi(q)} = \mathbf{0}, \mathbf{\Psi(y,q)} = \mathbf{0},\ \textbf{and}\ \mathbf{\Gamma(q,z)} = \mathbf{0}\}$ and the regular configuration space is $\tilde{X}^c = \{\mathbf{x} \in X^c : q_5 \neq 0, \sin(q_4 - q_2) \neq 0,\ \textbf{and}\ \sin q_2 \neq 0\}$. Thus, there are eight disjoint, maximal, path connected, singularity free components,

$$
\begin{aligned}
\tilde{X}_1^c &= \{\mathbf{x} \in X^c : q_5 > 0, \sin(q_4 - q_2) > 0, \sin q_2 > 0\} \\
\tilde{X}_2^c &= \{\mathbf{x} \in X^c : q_5 > 0, \sin(q_4 - q_2) > 0, \sin q_2 < 0\} \\
\tilde{X}_3^c &= \{\mathbf{x} \in X^c : q_5 > 0, \sin(q_4 - q_2) < 0, \sin q_2 < 0\} \\
\tilde{X}_4^c &= \{\mathbf{x} \in X^c : q_5 > 0, \sin(q_4 - q_2) < 0, \sin q_2 > 0\} \\
\tilde{X}_5^c &= \{\mathbf{x} \in X^c : q_5 < 0, \sin(q_4 - q_2) > 0, \sin q_2 > 0\} \\
\tilde{X}_6^c &= \{\mathbf{x} \in X^c : q_5 < 0, \sin(q_4 - q_2) > 0, \sin q_2 < 0\} \\
\tilde{X}_7^c &= \{\mathbf{x} \in X^c : q_5 < 0, \sin(q_4 - q_2) < 0, \sin q_2 < 0\} \\
\tilde{X}_8^c &= \{\mathbf{x} \in X^c : q_5 < 0, \sin(q_4 - q_2) < 0, \sin q_2 > 0\}
\end{aligned}
\tag{60}
$$

3.8 Compound Manipulator Obstacle Avoidance Using Self-Motion Manifolds

An application of the redundant manipulator formulation presented is obstacle avoidance, through use of self-motion manifolds. This is illustrated with the compound manipulator of Section 3.7. Output point P is required to follow the trajectory $\mathbf{z}_d(t) = [z_{1d}(t) \quad z_{2d}(t)]^T$, $0 < t < 0.7$, as illustrated in Fig. 11(a), where $\mathbf{z}_d(t) = [2\cos(t + \pi/20) \quad \sin(t + \pi/20) - \sin(t - 2\pi/5)]^T$, $0 \le t < 0.7$. This can be achieved with the *nominal* generalized coordinate and input trajectories $\mathbf{q}_n(t) = [q_{1n}(t) \quad q_{2n}(t) \quad q_{3n}(t) \quad q_{4n}(t) \quad q_{5n}(t)]^T$ and $\mathbf{y}_n(t) = [q_{3n}(t) \quad q_{1n}(t) \quad q_{5n}(t)]^T$, where $q_{1n}(t) = -\sin(t + \pi/20) - \sin(t - 2\pi/5)$, $q_{2n}(t) = t + \pi/20$, $q_{3n}(t) = \cos(t + \pi/20) + \cos(t - 2\pi/5)$, $q_{4n}(t) = t - 2\pi/5$, and $q_{5n}(t) = 1$, which is in component $\tilde{X}_4^c$ of Eq. (60). A circular obstacle with radius r = 0.2 m, centered at (0.86m,0.4m) in the plane of Fig. 11(b), is to be avoided by link 2 in achieving the desired output trajectory $\mathbf{z}_d(t)$.

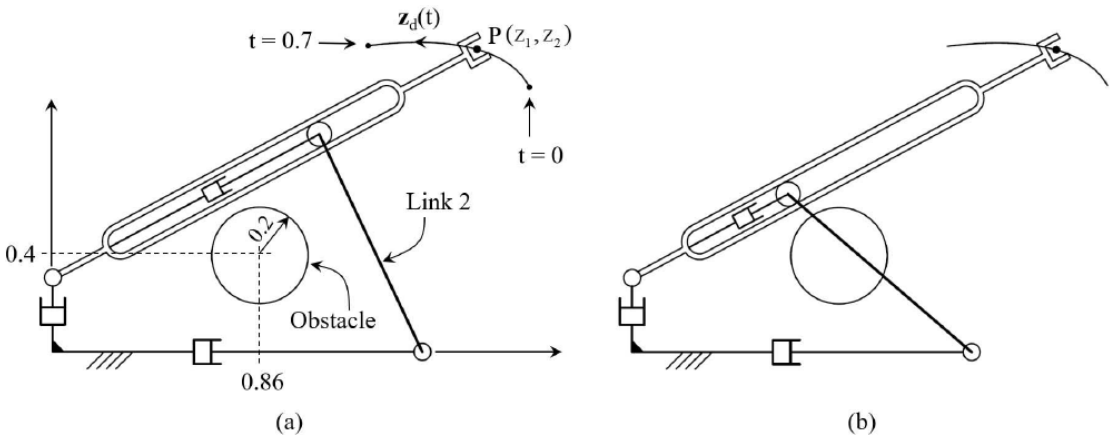

Figure 11 (a) Desired Output Trajectory $\mathbf{z}_d(t)$ and Obstacle; (b) Penetration of Obstacle by Link 2

The following algorithm is used to achieve the desired output trajectory, while avoiding collisions between the obstacle and link 2:

(1) On a grid t_i, $0 \le t_i \le 0.7$, at t_1 no collision exists, as shown in Fig. 11(a), so $\mathbf{q}_n(t_1)$ is a valid configuration. Therefore, set $\mathbf{q}_1 = \mathbf{q}_n(t_1)$.

(2) At step t_k, $k \ge 2$, determine if the nominal configuration $\mathbf{q}_n(t_k)$ produces interference between the obstacle and link 2. When checking interference, link 2 is regarded as a line segment with zero thickness.

(2a) If no interference occurs, set $\mathbf{q}_k = \mathbf{q}_n(t_k)$ and proceed to step t_{k+1}, repeating step **(2).**

(2b) If interference occurs, as in Fig. 11(b), proceed to step **(3).**

(3) Since $\mathbf{q}_n(t_k)$ produces interference, a new configuration on the self-motion manifold defined by $\bar{\mathbf{z}} = \mathbf{z}_d(t_k)$ is to be determined that yields no penetration of the obstacle by link 2. To do so, the one-dimensional self-motion mapping algorithm of Section 3.6 is used, starting from $\bar{\mathbf{q}} = \mathbf{q}_n(t_k)$. There are two possible directions to map the self-motion manifold, starting from $\bar{\mathbf{q}}$, namely v and $-v$.

(3a) March along the self-motion manifold in direction v with step h, starting from $\bar{\mathbf{q}}$, generating $\mathbf{q}^i(v^i, \bar{\mathbf{z}})$ until finding the first $\mathbf{q}^j(v^j, \bar{\mathbf{z}})$ that does not produce interference. This means that the obstacle is just contacted for some configuration $\mathbf{q}^*(v^*, \bar{\mathbf{z}})$ between $\mathbf{q}^j(v^j, \bar{\mathbf{z}})$ and $\mathbf{q}^{j-1}(v^{j-1}, \bar{\mathbf{z}})$. The configuration $\mathbf{q}^*(v^*, \bar{\mathbf{z}})$ is estimated by returning to $\mathbf{q}^{j-1}(v^{j-1}, \bar{\mathbf{z}})$ and advancing toward $\mathbf{q}^j(v^j, \bar{\mathbf{z}})$ using a finer step h/10, until interference does not occur.

(3a1) If index i exceeds a preset maximum number of steps (i_{max}) while marching along the manifold in the direction of v without finding an interference-free configuration, abort the mapping and proceed to step **(3b).**

(3a2) If $\left\| \mathbf{q}_{k-1} - \mathbf{q}^*(v^*, \bar{\mathbf{z}}) \right\| < \text{Tol}$, with tolerance Tol, the **q** trajectory is regarded as continuous. In that case, set $\mathbf{q}_k = \mathbf{q}^*(v^*, \bar{\mathbf{z}})$ and proceed to the next time-step t_{k+1}, repeating **(2).** Otherwise, proceed to step **(3b).**

(3b) Proceed as in step **(3a),** but marching in direction $-\mathrm{v}$. If this step generates a valid $\mathbf{q}_k$, proceed to step t_{k+1}, repeating step **(2).** If this sequence of steps fails to yield a valid $\mathbf{q}_k$, the desired output trajectory $\mathbf{z}_d(t)$ is infeasible, and the algorithm ends.

The foregoing algorithm generates a sequence of configurations $\{\mathbf{q}_1, \mathbf{q}_2, \mathbf{q}_3 \ldots\}$ that approximates a continuous trajectory in **q** space, which generates the desired output trajectory $\mathbf{z}_d(t)$. The result of executing this algorithm to track the output trajectory $\mathbf{z}_d(t)$ is shown in Fig. 12, as trajectories of $q_i(t)$. Trajectories shown as continuous lines are obtained by the proposed algorithm, while trajectories shown as dashed lines are the nominal $\mathbf{q}_n(t)$ that leads to penetration of the obstacle. Both trajectories coincide until approximately $t = 0.45$, after which collision occurs and link 2 remains in contact with the obstacle. Having the desired $\mathbf{q}(t_i)$ trajectory, Eq. (55) is solved to obtain the desired input trajectory $\mathbf{y}(t_i)$.

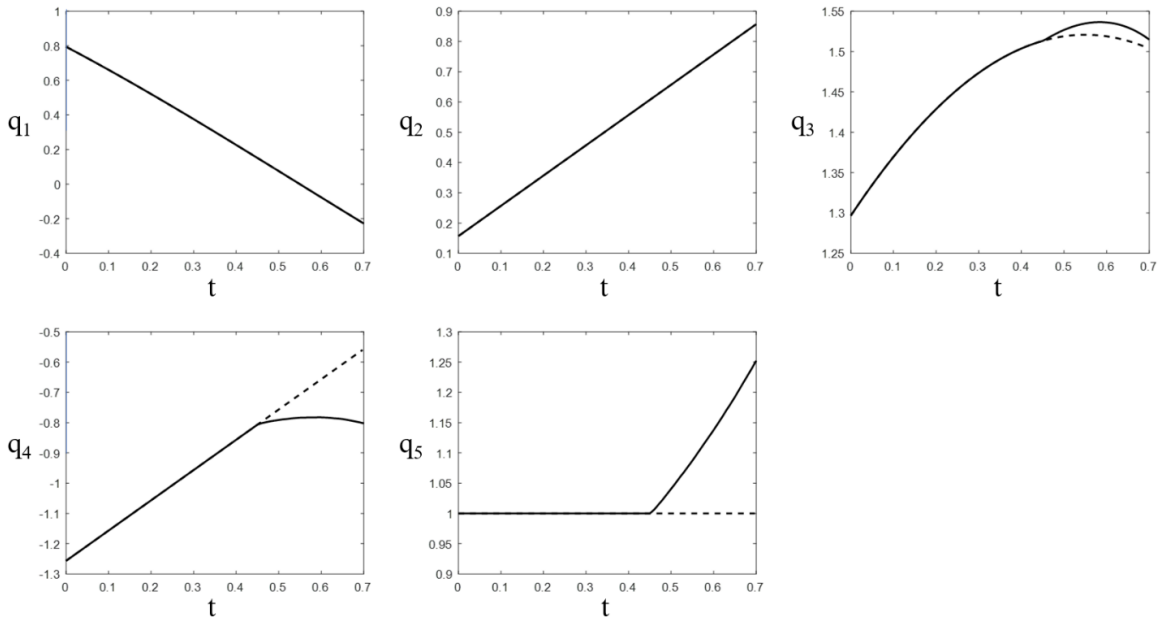

Figure 12 Evolution of **q** for the Nominal Trajectory (dashed line) and the Collision-Free Trajectory Obtained by the Foregoing Algorithm (continuous line).

The average CPU time required to run the foregoing algorithm and obtain the collision-free trajectory was 0.1 sec, using the same computer used for the 7R manipulator of Section 2.7. The algorithm was run with the following parameters:

(a) Maximum number i_{max} of steps marching along self-motion manifold when trying to find an interference-free configuration: 50

(b) Tolerance Tol to consider the sequence $\mathbf{q}_k$ as a continuous trajectory: 0.05

(c) Step size on the interval $0 \le t_i \le 0.7$: 0.01

(d) Step h used to map the self-motion manifold: 0.01

(e) Tolerance used in the iterative computation of **h** and **B** according to Appendix A, during mapping of the manifolds, according to Section 3.6: 0.0001.

(f) Maximum number of non-converging iterations to compute **h** or **B** before reevaluating **U** and **V** and resetting the parameterization of self-motion manifolds ($v^0 = 0$) according to Section 3.6: 10 iterations.

4 Conclusions

The differentiable manifold formulation presented for kinematically redundant manipulators provides explicit parameterizations of manipulator regular configuration manifolds and self-motion manifolds at the configuration level, in contrast with problem-dependent algebraic manipulation and velocity-based methods in the literature. Whereas the differentiable manifold structure of nonredundant manipulator analysis reduces to a multivariable calculus implementation [1, 2], for redundant manipulators, a much deeper differential geometric insight is provided into redundant manipulator kinematics. The distinctly different character of serial and non-serial redundant manipulators, called compound manipulators, is highlighted using examples with analytical and computational analysis of their characteristics. Computational methods for implementation of manifold parameterizations are shown to be practical and efficient in characterizing set-valued inverse kinematic mappings and enabling applications such as obstacle avoidance on maximal, disjoint, singularity free, path connected components of manipulator regular configuration space. As shown in [1, 2], computations required for their implementation can be carried out in real-time on modern high-speed microprocessors. Finally, differentiation of manifold configuration parameterizations yields set-valued velocity and acceleration inverse kinematic mappings that are needed for manipulator dynamics and control.

References

1 Haug, E.J., 2022, Manipulator Kinematics and Dynamics on Differentiable Manifolds: Part I Kinematics, Journal of Computational and Nonlinear Dynamics, Vol. 17, p. 021002.

2 Haug, E.J., 2022, Manipulator Kinematics and Dynamics on Differentiable Manifolds: Part II Dynamics, Journal of Computational and Nonlinear Dynamics, Vol. 17, p. 021003.

3 Chiaverine, S., Oriolo, G., and Maciejewski, A.A., 2016, Redundant Robots, Springer Handbook on Robotics, pp. 221-242.

4 Luces, M., Mills, J.K., and Benhabib, B., 2017, A Review of Redundant Parallel Kinematic Manipulators, J Intel Robot Sys, Vol. 86, pp. 175-198.

5 Muller, A, and Hufnagel, T, 2012, Model-Based Control of Redundantly Actuated parallel manipulators in Redundant Coordinates, Rob. Auton. Sys., Vol 64, No. 4, pp 563-571.

6 Burdick, J.W., 1989, On the Inverse Kinematics of Redundant Manipulators: Characterization of the Self-Motion Manifolds, Proceedings, 1989 IEEE Int. Conf. Robot Automation, Scottsdale AZ, pp264-270.

7 Lee, S., and Bejczy, A.K., 1991, Redundant Arm Kinematic Control Based on Parameterization, Proc. of the 1991 IEEE Int. Conf. on Robotics and Automation, Sacramento, CA, pp. 458-465.

8 Luck, C.L., and Lee, S., 1995, Topology-Based Analysis for Redundant Manipulators under Kinematic Constraints, Proceedings, 34th IEEE Conf. on Design and Control, New Orleans, pp.1603-1608.

9 DeMers, D., and Kreutz-Delgado, K., 1996, Canonical Parameterization of Excess Motor Degrees of Freedom with Self-Organizing Maps, IEEE Transactions n Neural Networks, Vol. 7, No. 1, pp. 43-55.

10 Shimizu, M., Kaleuya, H., Yoon, W-K, and Kitagaki, K., 2008, Analytical Inverse Kinematic Computation of 7-DOF Redundant Manipulators with Joint Limits and its Application to Redundancy Resolution, IEEE Transactions on Robotics, Vol. 24, No. 5, pp. 1131-1142.

11 Fari, C., Ferreira, F., Erlhagen, W., Monteiro, S., and Bicho, E., 2018, Position-based kinematics foe 7-DOF serial manipulators with global configuration control, joint limit, and singularity avoidance, Mechanism and Machine Theory, Vol. 121, pp. 317-334.

12 Wang, Y., Zhao, C., Wang, X., Zhang, P., and Liu, H., 2021, Inverse Kinematics of 7-DOF Spraying Robot with 4R 3-DOF Non-spherical Wrist, J. of Intel. & Rob. Sys., Vol. 101, No. 68.

13 Gosselin, C., and Schreiber, L.-T., 2018, Redundancy in Parallel Mechanisms: A Review, Applied Mechanics Reviews, Vol. 70, p. 010802.

14 Guillemin, V., and Pollack, A., 1974, Differential Topology, AMS Chelsea Publishing, Providence, RI.

15 Corwin, L.J., and Szczarba, R.H., 1982, Multivariable Calculus, Marcel Dekker, New York.

16 Mendelson, B., 1962, Introduction to Topology, Allyn and Bacon, Boston.

17 Atkinson, K.E.,1989, An Introduction to Numerical Analysis, Second Ed., Wiley, New York.

18 Hirsch, M.W., 1976, Differential Topology, Springer-Verlag, New York.

19 Jazar, R.N., 2010, Theory of Applied Robotics, Springer, Boston.

20 Peidro, A., Reinoso, O., Gil, A., Marín, J. M., and Paya, L., 2018. A method based on the vanishing of self-motion manifolds to determine the collision-free workspace of redundant robots, Mechanism and Machine Theory, Vol. 128, pp. 84-109.

21 Lee, H. Y., and Liang, C. G., 1988, Displacement analysis of the general spatial 7-link 7R mechanism. Mechanism and machine theory, Vol. *23*, No. 3, pp.219-226.

22 Haug, E.J., 2021, Multibody Dynamics on Differentiable Manifolds, Journal of Computational and Nonlinear Dynamics, Vol. 16, p. 041003.

Appendix A: Computation of $\mathbf{h}(\mathbf{v},\mathbf{z})$ and $\mathbf{B}(\mathbf{v},\mathbf{z})$

While vector and matrix functions $\mathbf{h}(\mathbf{v},\mathbf{z})$ and $\mathbf{B}(\mathbf{v},\mathbf{z})$ for compound redundant manipulators are shown to exist and be differentiable functions of **v** and **z**, the derivation does not show how to evaluate them. Since they are central to implementing inverse kinematic, velocity, and acceleration analysis, numerical methods for their evaluation are needed.

At $\bar{\mathbf{x}} \in \tilde{X}^c$, $\mathbf{B}(\bar{\mathbf{v}},\bar{\mathbf{z}}) = \left(\mathbf{\Lambda}_\mathbf{q}(\mathbf{q}(\bar{\mathbf{v}},\bar{\mathbf{z}}),\bar{\mathbf{z}})\mathbf{U}\right)^{-1} = \left(\mathbf{U}^T\mathbf{U}\right)^{-1}$ is numerically evaluated. For $(\mathbf{v}^i,\mathbf{z}^i)$ at time t^i, $\mathbf{B}(\mathbf{v}^i,\mathbf{z}^i)$ must satisfy Eq. (48), in the form $\bar{\mathbf{R}} \equiv \left(\mathbf{\Lambda}_\mathbf{q}(\mathbf{q}(\mathbf{v}^i,\mathbf{z}^i),\mathbf{z}^i)\mathbf{U}\right)\mathbf{B}(\mathbf{v}^i,\mathbf{z}^i) - \mathbf{I} = \mathbf{0}$. With an approximation $\mathbf{B}^{(1)} \approx \mathbf{B}(\mathbf{v}^{i-1},\mathbf{z}^{i-1})$ of the solution and suppressing arguments $(\mathbf{v}^i,\mathbf{z}^i)$ since they do not change in the iterative process for $\mathbf{B}(\mathbf{v}^i,\mathbf{z}^i)$, a matrix version of *Newton-Raphson iteration* [22] is defined by $\left(\mathbf{\Lambda}_\mathbf{q}\mathbf{U}\right)\Delta\mathbf{B}^{(j)} = -\bar{\mathbf{R}}^{(j)} = -\mathbf{\Lambda}_\mathbf{q}\mathbf{U}\mathbf{B}^{(j)} + \mathbf{I}$, where (j) denotes

iteration number. Since the matrix $\mathbf{\Lambda_q U}$ need not be inverted with great precision for use in the Newton-Raphson process [17] and $\mathbf{B}^{(j)} \approx \left(\mathbf{\Lambda_q U}\right)^{-1}$, $\Delta\mathbf{B}^{(j)} = -\mathbf{B}^{(j)}\mathbf{\Lambda_q U B}^{(j)} + \mathbf{B}^{(j)}$ and $\mathbf{B}^{(j+1)} = \mathbf{B}^{(j)} + \Delta\mathbf{B}^{(j)}$. This yields the iterative algorithm

$$\begin{aligned} \mathbf{B}^{(j+1)} &= 2\mathbf{B}^{(j)} - \mathbf{B}^{(j)}\mathbf{\Lambda_q U B}^{(j)}, \quad j = 1, 2, \cdots, \\ &\text{until } \left\| \mathbf{\Lambda_q U B}^{(j+1)} - \mathbf{I} \right\| \le \text{Btol} \end{aligned} \tag{61}$$

where Btol is a specified error tolerance. This is an efficient computation, requiring only matrix multiplication.

While $\mathbf{h}(\mathbf{v}^i\mathbf{z}^i)$ cannot be analytically determined, it can be evaluated as accurately as desired using Newton-Raphson iteration to solve Eq. (43) for $\mathbf{u} = \mathbf{h}(\mathbf{v}^i, \mathbf{z}^i)$, with $\mathbf{\Lambda_u}\Delta\mathbf{u}^{(j)} = -\mathbf{\Lambda_q U}\Delta\mathbf{u}^{(j)} = -\mathbf{B}^{-1}\Delta\mathbf{u}^{(j)} = -\mathbf{\Lambda}(\bar{\mathbf{q}} + \mathbf{V v} - \mathbf{U u}^{(j)}, \mathbf{z})$. The solution is $\Delta\mathbf{u}^{(j)} = \mathbf{B\Lambda}(\bar{\mathbf{q}} + \mathbf{V v} - \mathbf{U u}^{(j)}, \mathbf{z})$ and $\mathbf{u}^{(j+1)} = \mathbf{u}^{(j)} + \Delta\mathbf{u}^{(j)}$. This yields the iterative algorithm

$$\begin{aligned} \mathbf{u}^{(j+1)} &= \mathbf{u}^{(j)} + \mathbf{B\Lambda}(\bar{\mathbf{q}} + \mathbf{V v} - \mathbf{U u}^{(j)}, \mathbf{z}), \quad j = 1, 2, ... \\ &\text{until } \left\| \mathbf{\Lambda}(\bar{\mathbf{q}} + \mathbf{V v} - \mathbf{U u}^{(j+1)}, \mathbf{z}) \right\| \le \text{utol} \end{aligned} \tag{62}$$

where utol is a specified error tolerance. Since the Newton-Raphson method does not require an exact Jacobian, the matrix **B** is held constant throughout the process. This is an efficient computation, requiring only matrix multiplication.

The foregoing computations may be adapted to the less complex case of kinematically redundant serial manipulators of Section 2 by changing $\mathbf{\Lambda_q}(\mathbf{q}, \mathbf{z})$ to $\mathbf{G}'(\mathbf{y})$.

Appendix B Serial Manipulator Inverse Dynamics

Differentiating Eq. (15) with respect to time and suppressing arguments, $\dot{\mathbf{y}} = \mathbf{V}\dot{\mathbf{v}} - \mathbf{U}\left(\mathbf{h}_\mathbf{v}\dot{\mathbf{v}} + \mathbf{h}_\mathbf{z}\dot{\mathbf{z}}\right)$. Substituting from Eqs. (18),

$$\begin{aligned} \dot{\mathbf{y}} &= \mathbf{V}\dot{\mathbf{v}} - \mathbf{UB}(\mathbf{y})\mathbf{G}'\mathbf{V}\dot{\mathbf{v}} + \mathbf{UB}(\mathbf{y})\dot{\mathbf{z}} \\ &= \left(\mathbf{D}(\mathbf{y})\mathbf{V}\dot{\mathbf{v}} + \mathbf{UB}(\mathbf{y})\dot{\mathbf{z}}\right)_{\left|_{\mathbf{y}=\bar{\mathbf{y}}+\mathbf{Vv}-\mathbf{Uh}(\mathbf{v},\mathbf{z})}\right.} \end{aligned} \tag{63}$$

Where $\mathbf{D}(\mathbf{y}) \equiv \left(\mathbf{I} - \mathbf{UB}(\mathbf{y})\mathbf{G}'(\mathbf{y})\right)_{\left|_{\mathbf{y}=\bar{\mathbf{y}}+\mathbf{Vv}-\mathbf{Uh}(\mathbf{v},\mathbf{z})}\right.}$. Equation (63) is a $2(n-m)$ parameter inverse kinematic velocity mapping, for arbitrary $\mathbf{v}$ and $\dot{\mathbf{v}}$. Note that the redundant manipulator literature that works only at the velocity level misses half of these parameters; namely **v**.

Differentiating Eq. (63) with respect to time,

$$\begin{aligned} \ddot{\mathbf{y}} &= \mathbf{D}(\mathbf{y})\mathbf{V}\ddot{\mathbf{v}} + \mathbf{UB}(\mathbf{y})\ddot{\mathbf{z}} - \mathbf{U}\left(\mathbf{B}(\mathbf{y})\hat{\mathbf{G}}'\mathbf{V}\hat{\dot{\mathbf{v}}}\right)_\mathbf{y}\dot{\mathbf{y}} \\ &\quad - \mathbf{UB}(\mathbf{y})\left(\mathbf{G}'(\mathbf{y})\mathbf{V}\hat{\dot{\mathbf{v}}}\right)_\mathbf{y}\dot{\mathbf{y}} + \mathbf{U}\left(\mathbf{B}(\mathbf{y})\hat{\dot{\mathbf{z}}}\right)_\mathbf{y}\dot{\mathbf{y}} \end{aligned} \tag{64}$$

To evaluate terms of the form $\left(\mathbf{B}(\mathbf{y})\hat{\mathbf{a}}\right)_\mathbf{y}$, Eq. (17) is written in the form $\mathbf{G}'(\mathbf{y})\mathbf{UB}(\mathbf{y}) = \mathbf{I}$ or, with **a** constant, $\mathbf{G}'(\mathbf{y})\mathbf{UB}(\mathbf{y})\mathbf{a} = \mathbf{a}$. Differentiating this identity with respect to **y**,

$\left(\mathbf{G}'(\mathbf{y})\mathbf{U}\hat{\mathbf{B}}\hat{\mathbf{a}}\right)_{\mathbf{y}} + \mathbf{G}'(\mathbf{y})\mathbf{U}\left(\mathbf{B}(\mathbf{y})\hat{\mathbf{a}}\right)_{\mathbf{y}} = \mathbf{0}$. Using Eq. (17), $\left(\mathbf{B}(\mathbf{y})\hat{\mathbf{a}}\right)_{\mathbf{y}} = -\mathbf{B}(\mathbf{y})\left(\mathbf{G}'(\mathbf{y})\mathbf{U}\hat{\mathbf{B}}\hat{\mathbf{a}}\right)_{\mathbf{y}}$, which is computable. Thus, for all $\mathbf{v}$, $\dot{\mathbf{v}}$, and $\ddot{\mathbf{v}}$, the inverse acceleration mapping of Eq. (64) is

$$\begin{aligned}\ddot{\mathbf{y}} = &\left(\mathbf{D}(\mathbf{y})\mathbf{V}\ddot{\mathbf{v}} + \mathbf{U}\mathbf{B}(\mathbf{y})\ddot{\mathbf{z}}\right)_{\left|\mathbf{y}=\bar{\mathbf{y}}+\mathbf{V}\mathbf{v}-\mathbf{U}\mathbf{h}(\mathbf{v},\mathbf{z})\right.}\\ &+\mathbf{U}\mathbf{B}(\mathbf{y})\begin{bmatrix}\left(\mathbf{G}'(\mathbf{y})\mathbf{U}\hat{\mathbf{B}}\hat{\mathbf{G}}'\mathbf{V}\dot{\hat{\mathbf{v}}}\right)_{\mathbf{y}}\\ -\left(\mathbf{G}'(\mathbf{y})\mathbf{V}\dot{\hat{\mathbf{v}}}\right)_{\mathbf{y}} - \left(\mathbf{G}'(\mathbf{y})\mathbf{U}\hat{\mathbf{B}}\dot{\hat{\mathbf{z}}}\right)_{\mathbf{y}}\end{bmatrix}\dot{\mathbf{y}}_{\left|\begin{matrix}\mathbf{y}=\bar{\mathbf{y}}+\mathbf{V}\mathbf{v}-\mathbf{U}\mathbf{h}(\mathbf{v},\mathbf{z})\\ \dot{\mathbf{y}}=\left(\mathbf{D}(\mathbf{y})\dot{\mathbf{v}}-\mathbf{U}\mathbf{B}(\mathbf{y})\dot{\mathbf{z}}\right)\end{matrix}\right.}\end{aligned} \tag{65}$$

The function $\mathbf{h}(\mathbf{v},\mathbf{z})$ and matrix $\mathbf{B}(\mathbf{y})$ in the foregoing are evaluated in Appendix A. Provided the choice of $\mathbf{v}$ assures $\begin{bmatrix}\mathbf{y}^{\mathrm{T}} & \mathbf{z}^{\mathrm{T}}\end{bmatrix}^{\mathrm{T}} \in \tilde{\mathrm{X}}_{\mathrm{i}}^{\mathrm{s}}$, the foregoing relations involve free parameters $\mathbf{v}$, $\dot{\mathbf{v}}$, and $\ddot{\mathbf{v}}$ that may be chosen to satisfy kinematic, dynamic, and control requirements.

Appendix C Compound Manipulator Inverse Dynamics

For inverse velocity analysis, the time derivative of Eq. (44) is, suppressing arguments, $\dot{\mathbf{q}} = \mathbf{V}\dot{\mathbf{v}} - \mathbf{U}\left(\mathbf{h}_{\mathbf{v}}\dot{\mathbf{v}} + \mathbf{h}_{\mathbf{z}}\dot{\mathbf{z}}\right)$. Substituting from Eqs. (49),

$$\begin{aligned}\dot{\mathbf{q}} &= \mathbf{V}\dot{\mathbf{v}} - \mathbf{U}\mathbf{B}(\mathbf{v},\mathbf{z})\left(\mathbf{\Lambda}_{\mathbf{q}}(\mathbf{q}(\mathbf{v},\mathbf{z}),\mathbf{z})\mathbf{V}\dot{\mathbf{v}} + \mathbf{\Lambda}_{\mathbf{z}}(\mathbf{q}(\mathbf{v},\mathbf{z}),\mathbf{z})\dot{\mathbf{z}}\right)\\ &= \mathbf{D}(\mathbf{v},\mathbf{z})\dot{\mathbf{v}} - \mathbf{U}\mathbf{B}(\mathbf{v},\mathbf{z})\mathbf{\Lambda}_{\mathbf{z}}(\mathbf{q}(\mathbf{v},\mathbf{z}),\mathbf{z})\dot{\mathbf{z}}\end{aligned} \tag{66}$$

where $\mathbf{D}(\mathbf{v},\mathbf{z}) \equiv \left(\mathbf{I} - \mathbf{U}\mathbf{B}(\mathbf{v},\mathbf{z})\mathbf{\Lambda}_{\mathbf{q}}(\mathbf{q}(\mathbf{v},\mathbf{z}),\mathbf{z})\right)\mathbf{V}$. From Eqs. (38), (44), and (66), $\dot{\mathbf{y}} = \mathbf{g}'(\mathbf{q})\dot{\mathbf{q}} = \mathbf{g}'(\bar{\mathbf{q}} + \mathbf{V}\mathbf{v} - \mathbf{U}\mathbf{h}(\mathbf{v},\mathbf{z}))\left(\mathbf{D}(\mathbf{v},\mathbf{z})\dot{\mathbf{v}} - \mathbf{U}\mathbf{B}(\mathbf{v},\mathbf{z})\mathbf{\Lambda}_{\mathbf{z}}(\mathbf{q}(\mathbf{v},\mathbf{z}),\mathbf{z})\dot{\mathbf{z}}\right)$, where $\mathbf{g}'(\mathbf{q})$ is given in Eq. (51). This is a $2(\mathrm{n}-\mathrm{m})$ parameter inverse kinematic velocity mapping, for arbitrary $\mathbf{v}$ and $\dot{\mathbf{v}}$ and associated $\mathbf{z}$ and $\dot{\mathbf{z}}$. The redundant manipulator literature that works only at the velocity level misses half of these parameters; namely $\mathbf{v}$.

Differentiating Eq. (66) with respect to time,

$$\begin{aligned}\ddot{\mathbf{q}} = &\mathbf{D}\ddot{\mathbf{v}} - \mathbf{U}\mathbf{B}\mathbf{\Lambda}_{\mathbf{z}}\ddot{\mathbf{z}} - \mathbf{U}\left(\mathbf{B}(\mathbf{v},\hat{\mathbf{z}})\left(\hat{\mathbf{\Lambda}}_{\mathbf{q}}\mathbf{V}\dot{\hat{\mathbf{v}}} + \hat{\mathbf{\Lambda}}_{\mathbf{z}}\dot{\hat{\mathbf{z}}}\right)\right)_{\mathbf{v}}\dot{\mathbf{v}}\\ &- \mathbf{U}\left(\mathbf{B}(\hat{\mathbf{v}},\mathbf{z})\left(\hat{\mathbf{\Lambda}}_{\mathbf{q}}\mathbf{V}\dot{\hat{\mathbf{v}}} + \hat{\mathbf{\Lambda}}_{\mathbf{z}}\dot{\hat{\mathbf{z}}}\right)\right)_{\mathbf{z}}\dot{\mathbf{z}}\\ &- \mathbf{U}\mathbf{B}\left(\mathbf{\Lambda}_{\mathbf{q}}(\mathbf{q},\hat{\mathbf{z}})\mathbf{V}\dot{\hat{\mathbf{v}}} + \mathbf{\Lambda}_{\mathbf{z}}(\mathbf{q},\hat{\mathbf{z}})\dot{\hat{\mathbf{z}}}\right)_{\mathbf{q}}\dot{\mathbf{q}}\\ &- \mathbf{U}\mathbf{B}\left(\mathbf{\Lambda}_{\mathbf{q}}(\hat{\mathbf{q}},\mathbf{z})\mathbf{V}\dot{\hat{\mathbf{v}}} + \mathbf{\Lambda}_{\mathbf{z}}(\hat{\mathbf{q}},\mathbf{z})\dot{\hat{\mathbf{z}}}\right)_{\mathbf{z}}\dot{\mathbf{z}}\end{aligned} \tag{67}$$

To obtain computable expressions for terms of the form $\left(\mathbf{B}(\mathbf{v},\hat{\mathbf{z}})\hat{\mathbf{a}}\right)_{\mathbf{v}}$ and $\left(\mathbf{B}(\hat{\mathbf{v}},\mathbf{z})\hat{\mathbf{a}}\right)_{\mathbf{z}}$, Eq. (48) is written as $\mathbf{\Lambda}_{\mathbf{q}}(\mathbf{q}(\mathbf{v},\mathbf{z}),\mathbf{z})\mathbf{U}\mathbf{B}(\mathbf{v},\mathbf{z}) = \mathbf{I}$ and multiplied on the right by a constant vector $\mathbf{a}$, yielding $\mathbf{\Lambda}_{\mathbf{q}}(\mathbf{q}(\mathbf{v},\mathbf{z}),\mathbf{z})\mathbf{U}\mathbf{B}(\mathbf{v},\mathbf{z})\mathbf{a} = \mathbf{a}$. Differentiating this equation with respect to $\mathbf{v}$ and $\mathbf{z}$, $\left(\mathbf{\Lambda}_{\mathbf{q}}(\mathbf{q},\hat{\mathbf{z}})\hat{\mathbf{b}}\right)_{\mathbf{q}}\mathbf{q}_{\mathbf{v}} + \mathbf{\Lambda}_{\mathbf{q}}\mathbf{U}\left(\mathbf{B}(\mathbf{v},\hat{\mathbf{z}})\hat{\mathbf{a}}\right)_{\mathbf{v}} = \mathbf{0}$ and $\left(\mathbf{\Lambda}_{\mathbf{q}}(\mathbf{q},\hat{\mathbf{z}})\hat{\mathbf{b}}\right)_{\mathbf{q}}\mathbf{q}_{\mathbf{z}} + \left(\mathbf{\Lambda}_{\mathbf{q}}(\hat{\mathbf{q}},\mathbf{z})\hat{\mathbf{b}}\right)_{\mathbf{z}} + \mathbf{\Lambda}_{\mathbf{q}}\mathbf{U}\left(\mathbf{B}(\hat{\mathbf{v}},\mathbf{z})\mathbf{a}\right)_{\mathbf{z}} = \mathbf{0}$, where $\mathbf{b} = \mathbf{U}\mathbf{B}\mathbf{a}$. Using Eqs. (48), (44), and (49), $\left(\mathbf{B}(\mathbf{v},\hat{\mathbf{z}})\hat{\mathbf{a}}\right)_{\mathbf{v}} = -\mathbf{B}\left(\mathbf{\Lambda}_{\mathbf{q}}(\mathbf{q},\hat{\mathbf{z}})\hat{\mathbf{b}}\right)_{\mathbf{q}}\left(\mathbf{I} - \mathbf{U}\mathbf{B}\mathbf{\Lambda}_{\mathbf{q}}\right)\mathbf{V}$

and $\left(\mathbf{B}(\hat{\mathbf{v}},\mathbf{z})\hat{\mathbf{a}}\right)_{\mathbf{z}} = -\mathbf{B}\left\{-\left(\boldsymbol{\Lambda}_{\mathbf{q}}(\mathbf{q},\hat{\mathbf{z}})\hat{\mathbf{b}}\right)_{\mathbf{q}}\mathbf{U}\mathbf{B}\boldsymbol{\Lambda}_{\mathbf{z}} + \left(\boldsymbol{\Lambda}_{\mathbf{q}}(\hat{\mathbf{q}},\mathbf{z})\hat{\mathbf{b}}\right)_{\mathbf{z}}\right\}$. Substituting these results into Eq. (67) yields an intricate, but computable, expression for

$$\ddot{\mathbf{q}} = \mathbf{Q}_{\mathrm{dd}}(\mathbf{v},\dot{\mathbf{v}},\ddot{\mathbf{v}},\mathbf{z},\dot{\mathbf{z}},\ddot{\mathbf{z}}) \tag{68}$$

for arbitrary values of $\mathbf{v},\dot{\mathbf{v}},$ and $\ddot{\mathbf{v}}$. Finally, differentiating $\dot{\mathbf{y}} = \mathbf{g}'(\mathbf{q})\dot{\mathbf{q}}$ yields

$$\ddot{\mathbf{y}} = \mathbf{g}'(\mathbf{q})\ddot{\mathbf{q}} + \left(\mathbf{g}'(\mathbf{q})\hat{\dot{\mathbf{q}}}\right)_{\mathbf{q}}\dot{\mathbf{q}} \tag{69}$$

which, with $\ddot{\mathbf{q}} = \mathbf{Q}_{\mathrm{dd}}\left(\mathbf{v},\dot{\mathbf{v}},\ddot{\mathbf{v}},\mathbf{z},\dot{\mathbf{z}},\ddot{\mathbf{z}}\right)$, defines the input coordinate acceleration, with $\mathbf{v},\dot{\mathbf{v}},$ and $\ddot{\mathbf{v}}$ arbitrary. Evaluation of the second term on the right of Eq. (69) requires some manipulation. From Eq. (51), $\mathbf{g}'(\mathbf{q}) = -\boldsymbol{\Psi}_{\mathbf{y}}^{-1}(\mathbf{g}(\mathbf{q}),\mathbf{q})\boldsymbol{\Psi}_{\mathbf{q}}(\mathbf{g}(\mathbf{q}),\mathbf{q})$ and

$$\begin{aligned}\left(\mathbf{g}'(\mathbf{q})\hat{\dot{\mathbf{q}}}\right)_{\mathbf{q}} &= -\left(\boldsymbol{\Psi}_{\mathbf{y}}^{-1}(\mathbf{g}(\mathbf{q}),\mathbf{q})\hat{\boldsymbol{\Psi}}_{\mathbf{q}}\hat{\dot{\mathbf{q}}}\right)_{\mathbf{q}} \\ &-\boldsymbol{\Psi}_{\mathbf{y}}^{-1}\left[\left(\boldsymbol{\Psi}_{\mathbf{q}}(\mathbf{y},\hat{\mathbf{q}})\hat{\dot{\mathbf{q}}}\right)_{\mathbf{y}}\mathbf{g}'(\mathbf{q}) + \left(\boldsymbol{\Psi}_{\mathbf{q}}(\hat{\mathbf{y}},\mathbf{q})\hat{\dot{\mathbf{q}}}\right)_{\mathbf{q}}\right]_{\underline{\mathbf{y}=\mathbf{g}(\mathbf{q})}}\end{aligned} \tag{70}$$

Differentiating the identity $\boldsymbol{\Psi}_{\mathbf{y}}(\mathbf{g}(\mathbf{q}),\mathbf{q})\boldsymbol{\Psi}_{\mathbf{y}}^{-1}(\mathbf{g}(\mathbf{q}),\mathbf{q})\hat{\mathbf{a}} = \hat{\mathbf{a}}$ with respect to $\mathbf{q}$,

$$\begin{aligned}&\left[\left(\boldsymbol{\Psi}_{\mathbf{y}}(\mathbf{y},\hat{\mathbf{q}})\hat{\mathbf{b}}\right)_{\mathbf{y}}\mathbf{g}'(\mathbf{q}) + \left(\boldsymbol{\Psi}_{\mathbf{y}}(\hat{\mathbf{y}},\mathbf{q})\hat{\mathbf{b}}\right)_{\mathbf{q}}\right]_{\mathbf{y}=\mathbf{g}(\mathbf{q})} \\ &+\boldsymbol{\Psi}_{\mathbf{y}}(\mathbf{g}(\mathbf{q}),\mathbf{q})\left(\boldsymbol{\Psi}_{\mathbf{y}}^{-1}(\mathbf{g}(\mathbf{q}),\mathbf{q})\hat{\mathbf{a}}\right)_{\mathbf{q}} = \mathbf{0}\end{aligned} \tag{71}$$

where $\mathbf{a} = \boldsymbol{\Psi}_{\mathbf{q}}(\mathbf{g}(\mathbf{q}),\mathbf{q})\dot{\mathbf{q}}$ and $\mathbf{b} = \boldsymbol{\Psi}_{\mathbf{y}}^{-1}(\mathbf{g}(\mathbf{q}),\mathbf{q})\mathbf{a}$. Thus,

$$\begin{aligned}&\left(\boldsymbol{\Psi}_{\mathbf{y}}^{-1}(\mathbf{g}(\mathbf{q}),\mathbf{q})\hat{\boldsymbol{\Psi}}_{\mathbf{q}}\hat{\dot{\mathbf{q}}}\right)_{\mathbf{q}} \\ &= -\boldsymbol{\Psi}_{\mathbf{y}}^{-1}(\mathbf{g}(\mathbf{q}),\mathbf{q})\left[\left(\boldsymbol{\Psi}_{\mathbf{y}}(\mathbf{y},\hat{\mathbf{q}})\hat{\mathbf{b}}\right)_{\mathbf{y}}\mathbf{g}'(\mathbf{q}) + \left(\boldsymbol{\Psi}_{\mathbf{y}}(\hat{\mathbf{y}},\mathbf{q})\hat{\mathbf{b}}\right)_{\mathbf{q}}\right]_{\mathbf{y}=\mathbf{g}(\mathbf{q})}\end{aligned} \tag{72}$$

and, with Eq. (70), the inverse acceleration mapping of Eq. (69) is evaluated.